Sugarcane biorefinery: Unlocking the potential of the pyrolytic process to convert waste biomasses into value-added products

Tarcísio Martins [a], Mirele Santana de Sá [a], Wenes Ramos Silva [a], Caroline Carriel Schmitt [b], Renata Moreira [c], Klaus Raffelt [b], Nicolaus Dahmen [b], Alberto Wisniewski Jr [a,*]

[a] Petroleum and Energy from Biomass Research Group (PEB), Department of Chemistry, Federal University of Sergipe, São Cristóvão 49107-230, Sergipe, Brazil
[b] Institute of Catalysis Research and Technology, Karlsruhe Institute of Technology, 76344 Karlsruhe, Germany
[c] Laboratory of Bioenergy and Energy Efficiency, Institute for Technological Research, IPT, São Paulo 05508-901, São Paulo, Brazil

ARTICLE INFO

Keywords:
Sugarcane wastes
Biomass biorefinery
Pyrolysis process
Thermal analysis
Mass spectrometry
Value-added products

ABSTRACT

The sugarcane industry generates significant amounts of waste, such as bagasse (SCB) and sugarcane straw (SCS), which can be reused as raw materials to produce a wide range of renewable chemicals. This study, employing an approach that integrates kinetic studies and comprehensive product characterization, assessed the potential of pyrolysis to convert SCB and SCS into high-value-added inputs. Kinetic analysis revealed average activation energies (Ea) of ~139 kJ mol^{-1} and ~166 kJ mol^{-1} for SCB and SCS pyrolysis, respectively. Thermodynamic analysis, with ΔH values close to those of Ea, indicates low potential energy barriers and high viability of pyrolysis to recover bioenergy from the studied biomasses, as shown by ΔG values > 170 kJ mol^{-1}. SCB and SCS pyrolysis mainly produced pyrolytic liquids (58–63 wt%), with monomers, dimers, and trimers derived from lignin and holocellulose as main constituents. GC/MS analysis of the bio-oil revealed the predominance of phenolic compounds and sugar derivatives. These findings indicate that SCB and SCS generate pyrolytic liquids with similar compositions, suggesting potential as renewable industrial chemicals. This study highlights the possibility of expanding the sugarcane industry's product portfolio through sustainable management of these wastes.

1. Introduction

Biomass utilization as a source of energy and renewable chemicals has emerged as the most promising way to minimize dependence on petroleum and the impacts associated with its exploitation and consumption [1]. From an economic and industrial perspective, widely available and easily accessible biomass sources, such as agricultural processing industries waste, are the most advantageous raw materials for obtaining bio-products on a large scale, which may serve as industrial inputs [2,3]. In this way, the integration of biomass conversion processes into agro-industrial production sectors is a promising option for waste valorization, transforming traditional processing plants into an integrated system that is based on the concept of circular bioeconomy and aims to convert waste into renewable energy and value-added products – Biorefinery [4,5].

The sugarcane industry has a high potential to operate within the concept of a biorefinery, primarily due to the large volume of lignocellulosic waste generated during the production process, which can be used as raw material for a wide range of products [6]. The sugarcane industry is among the main sources of residual biomass in Brazil, which led the world's sugarcane production in 2023 with around 653 million tons produced [7]. It is estimated that during the sugarcane processing, to produce sugar and first-generation ethanol, about 27 % of bagasse (SCB) and 14 % of straw (SCS) are generated, which concentrates approximately 2/3 of all sugarcane energy content [8,9]. Furthermore, as they are lignocellulosic raw materials with a high content of cellulose and hemicellulose, SCB and SCS have a high potential to be converted into value-added products with a wide range of applications in energy transport and industrial sectors [10]. However, currently, the energy and chemical potential of these biomasses are underexploited by the sugarcane industry, thus, to explore the full potential of these residues for the production of biofuels and/or chemical inputs, it is necessary to investigate the applicability of efficient technologies for the conversion of residual biomass [11,12].

The conversion of biomass through pyrolysis is considered one of the most promising methods to produce value-added products [13].

* Corresponding author.
E-mail address: albertowj@academico.ufs.br (A. Wisniewski).

Pyrolysis consists of a thermal cracking process in an inert atmosphere, where organic matter is degraded by heat, producing gaseous products; solids (biochar); and a liquid product consisting of both an aqueous and an organic phase, called bio-oil [14]. Among them, biochar and bio-oil stand out as the most noteworthy bio-products, owing to their vast range of applications. Biochar is a product rich in recalcitrant carbon possessing a functionalized structure with a high polymerization degree, presenting promising properties to be used in high-performance energy storage devices development, for improving the quality of agricultural soils, among other applications [15]. Bio-oil, on the other hand, consists of a complex mixture formed mainly by oxygenated compounds, such as phenolic species, derived from the thermal cracking of lignin; sugar derivatives, originating from the polysaccharide matrix cleavage (cellulose and hemicellulose) and compounds from secondary cracking reactions, such as short-chain carboxylic acids, alcohols, furans, aldehydes, and ketones [16]. As it is a matrix rich in compounds of high industrial interest, bio-oil can be applied in different sectors of the economy through upgrading and refining, transforming into fuel or inputs for the chemical industry, reducing the demand for petrochemicals [17,18].

Understanding the composition of bio-oil is an important step for a more precise analysis of the potential applicability of this product [19]. Most studies focus on the use of gas chromatography (GC) techniques for the characterization of pyrolytic oils However, this analysis is limited to the speciation of the bio-oil volatile fraction, which may represent at most 50 % of the total composition of raw bio-oil derived from a lignocellulosic matrix [20]. Therefore, Ultra-High Resolution Mass Spectrometry (UHRMS) emerges as a powerful tool to complement the chemical speciation of polar, non-volatile, and high molecular weight structures, enabling comprehensive molecular characterization of pyrolytic oils [21,22].

Among the ionization techniques used for the UHRMS analysis of complex mixtures, electrospray ionization (ESI) and atmospheric pressure chemical ionization (APCI) have gained considerable attention for the analysis of pyrolytic oils derived from lignocellulosic matrices [23,24]. Depending on the ionization source and the mode of analysis used (positive or negative), different compounds tend to be preferentially ionized. Analysis of bio-oils using ESI in positive mode (ESI (+)) allows for greater ionization efficiency for basic nature compounds and sugar derivatives, through the formation of ions such as $[M+H]^+$ and $[M+Na]^+$, respectively [25]. Therefore, it is a powerful technique for the speciation of biomass polysaccharide matrix derivatives. When used in negative ionization mode, ESI allows for greater ionization efficiency of acidic compounds, mainly species containing carboxylic groups (COOH), which can suppress other species. To minimize the ion suppression effect, analysis using the APCI source in negative mode (APCI (–)) has been highly efficient for further speciation of acidic, aromatic, and low to medium polarity compounds, thus being effective for an efficient ionization of lignin derivatives [23,26,27].

In addition to the advanced characterization of the pyrolysis liquid product, it is necessary to understand the intrinsic nature of the conversion technology employed focusing on the production process optimization [28]. The determination of the kinetic and thermodynamic parameters involved in the pyrolytic process is an important step for the optimization and scalability of the thermal cracking technology, as well as assisting in the proposition of industrial systems for biomass conversion [29]. The kinetic study of pyrolysis is typically conducted through thermogravimetric analysis (TGA), where mathematical models allow for an estimation of the apparent activation energy (Ea) and other parameters involved in the reaction process [30]. Among the applicable models for estimating the activation energy of the pyrolysis process, the Flynn-Wall-Ozawa (FWO), Kissinger-Akahira-Sunose (KAS), and Starink (STK) models have been widely used for the kinetic analysis of residual biomass pyrolysis [31–33].

Considering the literature on the pyrolysis of sugarcane industry residues for bioenergy production, several studies have addressed a comparative analysis of the characteristics of products obtained during bagasse and straw pyrolysis or the kinetic parameters involved in the conversion process. Rodríguez-Machín et al. (2023) [34] conducted chemical characterization of bio-oils derived from SCB and SCS and observed that the volatile fraction of the liquid product showed a high content of carbohydrate derivatives and phenolic species. This finding corroborates the study by Barros et al. (2018) [35], which found that both SCB and SCS produce bio-oils with similar chemical composition, mainly consisting of phenolic compounds. Song et al. (2019) [36], in their study of the kinetics involved in the thermal degradation of sugarcane residues, observed that the pyrolysis of residual biomass occurred through the combined effects of multiple reaction mechanisms. Rueda-Ordóñez and Tannous (2015) [37], while studying the kinetics involved in the thermal decomposition of SCS, showed that the straw degrades through bidimensional diffusion mechanisms with activation energies ranging between 154 and 177 kJ mol^{-1}. Meanwhile, de Palma et al. (2019) [38] reported that the activation energy for the pyrolysis of SCB and SCS ranged between 175 kJ mol^{-1} and 200 kJ mol^{-1}, respectively.

However, despite the significant effort dedicated to the use of sugarcane bagasse and straw as raw materials to produce bio-derived inputs, the literature still lacks studies that correlate the kinetics of the pyrolysis process of these residues with the molecular characteristics of the pyrolytic products. Additionally, it is important to consider that the characteristics of sugarcane bagasse and straw can vary depending on the species of sugarcane processed and the growing conditions. This variation can result in slightly different products and processes depending on the mill producing and supplying the residues. Therefore, this study aims to obtain data to evaluate the potential of using the thermal conversion process of sugarcane industry residues. This will help implement the pyrolysis process in the sugarcane processing industry through a comprehensive analysis of the kinetics and molecular characteristics of the products from bagasse and straw pyrolysis. This will enable the sugarcane sector to diversify the portfolio of products.

2. Materials and methods

2.1. Physicochemical characterization of biomass

The sugarcane bagasse (SCB) and straw (SCS) used in this study were provided by a sugarcane mill located in the municipality of Iracemápolis, São Paulo, Brazil. Before being employed in the pyrolysis process, the raw materials were air-dried to reduce the residual moisture content of the samples to values close to 10 %. After drying, both SCB and SCS were subjected to milling to produce particles with sizes $\leq$ 2 mm. Subsequently, both biomasses were characterized to obtain data regarding physicochemical properties. Proximate analysis was performed according to ASTM D1762-84 standard methodology. Elemental analyses (CHN) of the received residues were conducted using a LECO CHN628 elemental analyzer, while the oxygen content was determined by difference on ash-free dry basis. The content determination of the biomass constituents (extractives, hemicellulose, cellulose, and lignin) was carried out through the deconvolution process of the derivatives curves of both biomasses' thermogravimetric analyses.

2.2. Thermogravimetric analysis

The thermogravimetric behaviors of SCB and SCS were determined using a Shimadzu TGA-50 thermogravimetric analyzer with a sensitivity of 0.001 mg. It was operated using a 75 μL platinum crucible in a nitrogen atmosphere at a flow rate of 50 mL min^{-1}. Initially, the SCB and SCS samples were subjected to ball milling for particle size homogenization (<150 μm), and then the biomasses were analyzed using approximately 10 mg of raw material. Before starting the temperature program, the equipment was purged with N_2 until mass stabilization. Both biomasses were heated from room temperature to 1000 °C using

four different heating rates (10, 15, 20, and 25 °C min ^{1}) to elucidate the different pyrolysis behaviors of the samples and enable the kinetic study. The lignocellulosic sample compositions were determined from the SCB and SCS derivative thermogravimetric curves (DTG), obtained at the different heating rates, through a progressive deconvolution procedure based on the parallel reactions model described by Kim et al. (2022) [39]. The statistical measure (R^2) was 0.99 for all four deconvolutions, indicating a good fit of the model with the experimental data.

2.3. Kinetic and thermodynamic study

The kinetic modeling of the degradation of SCB and SCS was carried out based on the results of the TGA analysis using the temperature range where the main mass loss zone of the biomass occurs. The mass loss data were converted into conversion units (α), defined by $\alpha = (m_i \quad m_t)/(m_i \quad m_f)$ where, m_i, m_t e m_f correspond to the initial sample mass, the mass at time t, and the final mass, respectively. The expression of the conversion rate (dα/dt) was determined using the generalized form of the kinetic equation combined with the Arrhenius equation, as presented in Eq. (1).

$$\frac{d\alpha}{dt} = A exp\left[\quad \left(\frac{E_a}{RT}\right) \right] f(\alpha) \tag{1}$$

Where A corresponds to the pre-exponential factor, Ea to the activation energy, R to the universal gas constant, T to the temperature (K) and f(α) indicates the kinetic mechanism function dependent on the α. Considering a constant heating ramp (βdT/dt), the term dα/dt can be expressed as βdα/dT. Thus, the conversion rate equation can be rearranged as follows:

$$\frac{d\alpha}{f(\alpha)} = \frac{A}{\beta} exp\left[\quad \left(\frac{E_a}{RT}\right) \right] dT \tag{2}$$

In integral form, Eq. (2) is expressed as:

$$g(\alpha) = \int_0^{\alpha} \frac{d\alpha}{f(\alpha)} = \frac{A}{\beta}\int_{T_0}^{T} exp\left[\quad \left(\frac{E_a}{RT}\right) \right] dT \tag{3}$$

The left side of Eq. (3) corresponds to the integral form of the reaction models, while the temperature integral (right side of Eq. (3)) does not have an exact analytical solution. Therefore, to describe pyrolysis kinetics, it is necessary to use approximate models [40]. In this study, the FWO, KAS, and STK isoconversional models were used to determine the activation energy (Ea) of the SCB and SCS thermal conversion process. Based on these models, Ea is calculated for each degree of conversion using the slope coefficient of a linear regression between a dependent variable X and an independent variable Y, derived from the linearization of the approximate solution of Eq. (3). The linearization equations and variables for each model applied are available at **Table S1**.

After determining the Ea values, the pre-exponential factor (A) and the thermodynamic parameters (ΔG, ΔH, and ΔS) for transitional state were estimated using the equations below, as described by Zhang et al. (2023) [41].

$$A_\alpha = \frac{\beta E_\alpha}{RT_p^2} Exp\left(\frac{E_\alpha}{RT_p}\right) \tag{4}$$

$$\Delta G_\alpha^* = E_\alpha + RT_\alpha ln\left(\frac{k_b T_\alpha}{A_\alpha h}\right) \tag{5}$$

$$\Delta H_\alpha^* = E_\alpha \quad RT_\alpha \tag{6}$$

$$\Delta S_\alpha^* = R\left[ln\left(\frac{A_\alpha h}{k_b T_\alpha}\right) \quad 1 \right] \tag{7}$$

Where T_p corresponds to the temperature (K) where the maximum degradation rate of the sample occurs, k_b is Boltzmann's constant (1,381 × 10 ^{23} J K ^{1}) and h is the Plank constant (6,626 × 10 ^{34} J s ^{1}).

2.4. Micro-scale pyrolysis experiments

The pyrolysis experiments of SCB and SCS were conducted using a micro-scale tubular reactor operating in tandem mode. The system consists of a borosilicate glass tube (500 mm × 4 mm) housed within two sequentially arranged electrically heated furnaces using Nickel-Chromium resistances, where each furnace has independent temperature control. The first furnace, responsible for the thermal cracking of the feedstock, operated at 500 °C. The second furnace operated at 350 °C, aiming to fractionate the liquid product of pyrolysis into two fractions, low and high molecular mass, LMM and HMM, respectively. An illustration of the microreactor is provided in the Supplementary Material (**Figure S1**).

Approximately 100 mg of biomass was introduced into the tube, supported with glass wool. The tube containing the feedstock was inserted into the heating system so that the biomass bed was arranged inside furnace 1. Before the heating started, the tube was purged for 2 min with nitrogen gas (N_2) at a flow rate of 5 mL min ^{1} for the complete removal of oxygen, which was maintained throughout the process. The procedure for operating the pyrolysis reactor, recovery, and determination of the yields of pyrolytic products was described in our previous work [42].

2.5. Characterization of pyrolysis products

2.5.1. Biochar characterization

The carbon (C), hydrogen (H), and nitrogen (N) content in the produced biochars were determined by CHN analysis using a LECO CHN628 analyzer (St. Joseph, MI, USA). The equipment was operated with helium (99.995 %) and oxygen (99.99 %), with a furnace temperature of 950 °C and post-combustion temperature of 850 °C. The system was calibrated with EDTA standard (41.0 % C, 5.5 % H, and 9.5 % N) using a mass range between 10 and 200 mg. The oxygen (O) content in the biochars was determined by difference, also considering the ash content present in the biocarbon samples, which was estimated based on the ash content present in the biomass ($Ash_{Feedstock}$) and the biochar yield obtained (Y_{BC}), as shown in Eq. (8).

$$Ash_{BC}(wt\%) = \frac{(Ash_{Feedstock} x M_{Feedstock})}{(Y_{BC} x M_{Feedstock})} = \frac{Ash_{Feedstock}}{Y_{BC}} \tag{8}$$

2.5.2. Characterization of the low molecular mass fraction of the liquid products by GC/MS

Due to the nature of LMM (non-condensable at 350 °C), constituted by a significant concentration of low molecular weight compounds and higher potential for volatilization, gas chromatography-mass spectrometry (GC/MS) analysis was exclusively applied to this fraction of the liquid product. The LMMs from SCB and SCS pyrolysis were subjected to the silylation reaction, employing N, O-bis(trimethylsilyl)trifluoroacetamide (BSTFA) as a derivatizing agent, to enhance the compounds volatilization, analysis sensitivity, and improve the detection of functionalized compounds. The final sample solutions were analyzed on a Thermo-Fisher Scientific GC/MS system model TRACE 1310/TSQ 9000 (Thermo-Fisher Scientific, Austin, TX, USA) equipped with a NA-5MS column (60 m x 0.25 mm; 0.25 μm). The derivatization procedure and operational conditions of the chromatographic system are detailed in Silva et al. (2022) [43]. Compounds identification was carried out by comparing the experimentally obtained mass spectra with spectra available in the NIST spectral library (version 2.73; 2017). For isomers with similar spectra, confirmation of identification was performed through a comparison of experimental retention indices, calculated using a standard of n-alkanes, with retention indices available in the literature.

2.5.3. Characterization of the liquid products by Ultra-High resolution mass spectrometry

The liquid fractions (LMM and HMM) from SCB and SCS pyrolysis were characterized by UHRMS using a Thermo-Fisher Scientific Exactive Plus Orbitrap system (Thermo-Fisher Scientific, Austin, TX, USA). LMM and HMM samples were diluted in tetrahydrofuran (HPLC grade) to obtain the final sample with a concentration of 300 μg ml ^{1}. Then, the analysis solutions were characterized by H-ESI(+) and APCI(–)–FT–Orbitrap MS. For the analysis by H-ESI(+), the following instrumental conditions were used: Sheat gas flow at 25 arbitrary units (a.u.), auxiliary gas temperature at 110 °C, S-Lens RF level at 65 %, capillary temperature at 320 °C, and spray voltage at + 3.8 kV. For analyses by APCI(–), the conditions were as follows: Sheat gas flow at 40 a.u., auxiliary gas flow at 10 a.u., vaporization temperature at 300 °C, S-Lens RF level at 70 %, capillary temperature at 320 °C, and spray current at 4 μA. Spectra were acquired in scan mode in the range of *m/z* 100 to 800, with 100 micro scans and a Full Width Half Maximum resolution (FWHM) of 140,000 (*m/z* 200). The final mass spectrum was obtained by subtracting the blank spectrum from the sample mass spectrum and processed using an advanced data processing approach.

The Xcalibur Qual Browser software was used to assign molecular formulas to the ions. At this stage, up to 10 possible molecular formulas were accepted for each *m/z* with an error lower than 3 ppm. Criteria for elemental composition assignment were: $^{12}C_{5\text{-}75}$, $^{13}C_{0\text{-}1}$, $^{1}H_{5\text{-}150}$, $^{16}O_{0\text{-}15}$, $^{14}N_{0\text{-}5}$, $^{23}Na_{0\text{-}1}$ (Only for H-ESI (+)), +1 charge for analysis using H-ESI (+), and –1 for APCI(–). The ions list with the molecular formulas assigned was transferred to Microsoft Excel and processed with an algorithm based on Visual Basic for Applications (VBA) programming language, which was employed to select the most probable molecular formula. To do so, the isotopic pattern of ^{13}C and Kendrick mass defects (tolerance ± 0.001) were evaluated to confirm the accuracy of elemental composition assignments.

3. Results and discussions

3.1. Biomass proximate and elemental analyses

The knowledge about the characteristics of the raw material to be processed plays an important role in the analysis of the thermal conversion potential of residual biomass into chemical feedstocks or bioenergy [44]. The results obtained from the characterization of sugarcane bagasse and straw through proximate and ultimate analysis are presented in Table 1.

The residual moisture content present in SCB and SCS was 8.75 % and 10.74 %, respectively. For thermal conversion processes, it is ideal for the moisture content in the feedstock to be lower or close to 10 %. The analyzed biomasses exhibited moisture levels that comply with this standard, indicating their suitability for use in the pyrolytic process [46]. Regarding volatile matter (VM) content, it was observed that both SCB and SCS exhibited high values (above 75 %). According to Silva et al. (2019) [47], the high percentage of VM implies a high potential for converting the raw material into renewable feedstocks via pyrolysis. VM and fixed carbon (FC) metrics also provide clues about the lignocellulosic composition of the material. In general, a higher FC content indicates a higher lignin content in the material, while a higher VM content suggests a higher cellulose and hemicellulose content [48,49]. The higher fixed carbon content in the straw (15.98 %) suggests that, compared to the bagasse (9.62 %), the SCS sample has a higher lignin content, while the SCB, due to its higher volatile content, has a higher percentage of polysaccharides. About the ash content, it was observed that, compared to the SCB sample, SCS has a higher content of inorganic materials. This result is consistent with the fact that straw is a residual biomass that is in greater contact with agricultural soil. This observation is aligned with information reported in the literature [38,50].

Table 1
Proximal and elemental properties of SCB and SCS biomass.

Parameter	SCB	SCS	SCB[d]	SCS[d]
Proximate Analysis (wt. %)				
Moisture	8.75 ± 0.24	10.74 ± 0.54	6.61 ± 2.37	7.16 ± 3.37
VM (dry basis)	87.05 ± 0.46	75.34 ± 0.84	82.16 ± 5.72	81.35 ± 5.54
Ash (dry basis)	3.33 ± 0.20	8.68 ± 0.14	5.13 ± 5.02	8.41 ± 2.48
FC[a] (dry basis)	9.62 ± 0.66	15.98 ± 0.75	12.72 ± 2.97	10.25 ± 5.44
Elemental Analysis (wt. %)				
C	43.26	42.24	44.82 ± 3.34	42.31 ± 1.66
H	6.95	6.65	5.93 ± 0.52	5.68 ± 0.24
N	0.41	0.47	0.43 ± 0.35	0.44 ± 0.17
O[b]	46.05	41.96	44.42 ± 3.81	43.68 ± 3.39
H/C molar ratio	1.93	1.89	1.60 ± 0.21	1.61 ± 0.10
O/C molar ratio	0.80	0.75	0.75 ± 0.12	0.78 ± 0.07
HHV (MJ kg ^{1})[c]	17.44	17.14	17.35 ± 1.45	17.24 ± 0.88

[a] Determined by the difference; [b] Determined by difference on ash-free basis; [c] Estimated based on the equation proposed by Noushabadi et al. (2021) [45]; [d] Average values reported by Najafi et al. (2023) [10].

From the elemental analysis of the biomass under study, it was observed that the carbon (C), hydrogen (H), nitrogen (N), and oxygen (O) contents found are similar to the values reported in the study by Najafi et al. (2023) [10]. Both samples, bagasse, and straw, were mainly composed of carbon and oxygen. The C and O contents in the SCB sample were approximately 43 % and 46 %, respectively, while in the SCS sample, the percentages for both elements were around ~ 42 %. The high amount of oxygen in the biomass is attributed to the presence of cellulose, hemicellulose, and lignin, which are the main components of lignocellulosic biomass [20]. Additionally, the lower oxygen concentration in the SCS, compared to the SCB, may occur due to a higher lignin content in this residual biomass [51]. This is consistent with assumptions made about the difference in the fixed carbon levels of the biomass under study.

The molar ratio of H/C can be used as an indicator of the degree of aromaticity of the biomass [52]. H/C values greater than 1.5 suggest that the matrix studied is composed of structures with naphthenic and/or aliphatic carbon chains. On the other hand, values below 1.0 indicate the predominance of aromatic carbon chains. For sugarcane industry residues, the molar ratios of H/C varied between 1.89 and 1.93, indicating that both bagasse and straw have a predominantly aliphatic nature. As for the O/C ratio, used as an indicator of the presence of oxygenated functional groups, it may be directly related to the lignocellulosic composition of the raw material. Straw presented a slightly lower O/C ratio than bagasse, with 0.75 for SCS and 0.80 for SCB. This suggests a higher concentration of lignin in this material, as lignocellulosic matrices with lower O/C ratios tend to have higher lignin content and lower holocellulose content [43]. The higher heating value (HHV) for both biomass samples under study was approximately 17 MJ kg ^{1}. This result is in agreement with the data available in the literature for this type of biomass and reveals that both SCB and SCS have high potential for bioenergy production [10].

3.2. Assessment of thermal degradation behavior

The results obtained from thermogravimetric analyses of sugarcane bagasse and straw samples using heating ramps of 10, 15, 20, and 25 °C min ^{1} is represented by the mass loss curves (TGA) and derivative mass loss (DTG) curves available in Fig. 1.

The TGA curves of the sugarcane residues exhibited a uniform thermal degradation pattern under the four different analysis conditions. This suggests that the heating rate did not have a significant impact on the degradation pattern but rather the reaction rates. This can be observed by the increase in DTG as the heating rate was increased. The thermogravimetric behavior of both biomass samples can be classified into 3 stages, namely: initial devolatilization (T≤150 °C), active pyrolysis (150 °C≤T≤700 °C), and char formation (T≥700 °C). During the initial devolatilization phase, a mass loss of ~ 9 % was observed for the SCB and about 11 % for the SCS. This first phase of the degradation

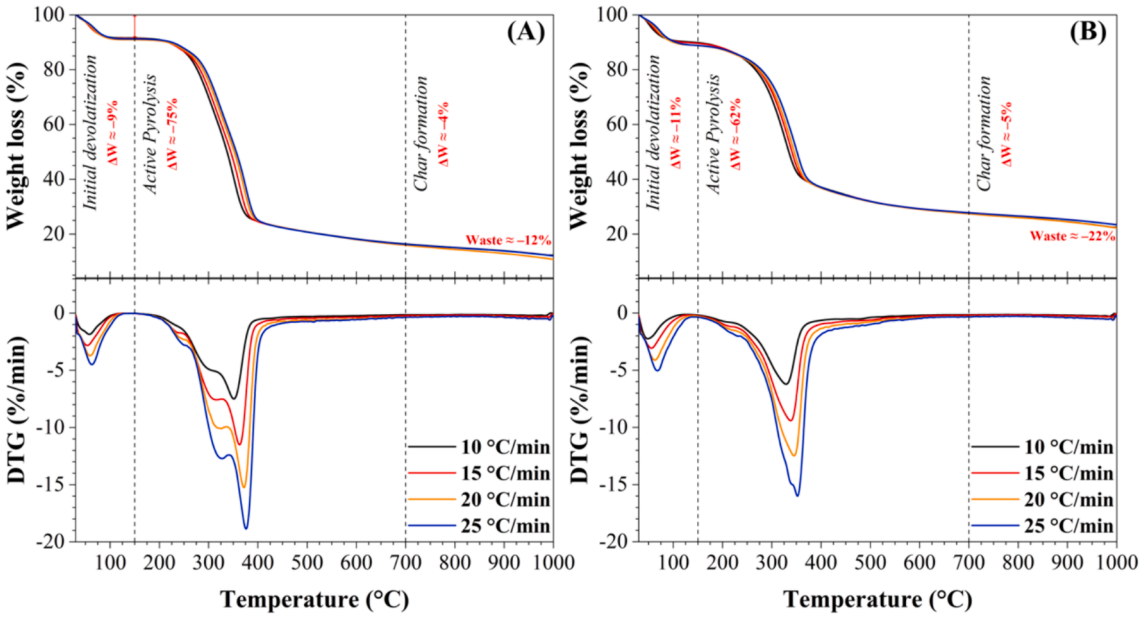

Fig. 1. TGA and DTG curves of the biomasses studied at heating rates of 10, 15, 20, and 25 °C min^{-1}: A) SCB and B) SCS.

process is associated with the release of residual moisture from the raw material and the volatilization of low molecular weight compounds [32]. The most significant mass losses were observed during the active pyrolysis phase, between 150 and 700 °C. According to Alves et al. (2023) [53], the active pyrolysis phase is characterized by the temperature range in which devolatilization and degradation of extractive components, hemicellulose, and cellulose occur, as well as partial decomposition of lignin, resulting in the release of volatiles. In this temperature range, a mass loss of approximately 75 % for SCB and 62 % for SCS was observed. The degradation percentages of the samples in this stage are consistent with the volatile material content presented in Table 1. The residue content in the analysis of SCB was ~12 %, while in the SCS analysis was 22 %. The higher amount of residue for sugarcane straw, compared to bagasse, corroborates the higher ash and fixed carbon content present in the SCS sample. Furthermore, this result is in line with the hypothesis regarding the higher lignin content in the straw, as it is the most stable polymer in biomass, its decomposition occurs slowly over a wide temperature range (160–900 °C), contributing significantly to the char formation stage and the final residue percentage in the TGA analysis [54].

Evaluating the active pyrolysis stage on DTG curves, distinct profiles were observed between the assessed biomass samples. Higher rates of thermal degradation were observed in the SCB sample compared to SCS, which may be related to a higher cellulose content in this material [55]. In sugarcane bagasse, the mass losses observed in this region occur through overlapping multiple thermal degradation events, where at least three events can be identified from the peaks/shoulders on the DTG curve in Fig. 1**–A**. The first mass loss event, occurring at ~ 230 °C, was attributed to the decomposition process of extractive components, such as soluble sugars [56]. The second peak, observed at ~ 300 °C, can be associated with the degradation process of hemicellulose [57], while the third event, showing the highest decomposition rate, occurred at around 350 °C and was attributed to cellulose decomposition [39]. Due to the slow degradation of lignin occurring at temperatures in the range of 160 to 900 °C, visualization of the corresponding decomposition event was difficult. In the SCS sample DTG curve (Fig. 1**–B**), it was not possible to distinguish the different mass loss events due to the total overlap of degradation peaks of lignocellulosic polymers, resulting in a single broadened degradation peak, with the maximum degradation rate occurring at ~ 330 °C. This result may indicate significant differences between the hemicellulose, cellulose, and lignin contents present in bagasse and straw. To verify this hypothesis, the lignocellulosic composition of the biomass under study was estimated through the deconvolution process of the DTG curves obtained at the different heating rates used.

For compositional analysis, only the active pyrolysis zone was considered, as no significant mass losses were observed after the temperature of 700 °C. For this analysis, the mass loss data of both biomass occurring in this temperature range were normalized to conversion units (α), and conversion rates (dα/dt) were calculated. The experimental curves obtained from TGA analysis of the studied biomass were simulated considering the individual contribution of 4 constituents, namely: extractives, hemicellulose, cellulose, and lignin. The parameters obtained in the data modeling stage are available in **Table S2** of the supplementary materials. The method developed by Kim et al. (2022) [39] satisfactorily reproduced the thermal degradation process of sugarcane bagasse and straw biomasses, showing fitting errors lower than 2.75 % for the dα/dt curves and 1.75 % for the conversion curves.

Analyzing the individual contributions of the biomass components to the conversion curve profiles obtained from the analysis at 10, 15, 20, and 25 °C min^{-1}, available in **Figure S2**, it was possible to access the degradation profile of each constituent of the studied biomass separately. The extractives degradation occurred in the temperature range between 150 and 275 °C. Hemicellulose was degraded in a temperature range ranging from 200 to 375 °C, with the maximum degradation rate observed at 295 °C for bagasse conversion and 285 °C for straw. Cellulose degradation occurred between 250 and 400 °C, with maximum conversion rates occurring at 350 °C for the SCB sample and 330 °C for SCS. As for lignin, its degradation was gradual across the temperature range between 150 and 700 °C, reaching the maximum rate at around 400 °C. The temperature ranges at which biomass constituents degrade are consistent with literature data [58–60].

The results of the lignocellulosic composition estimation for sugarcane bagasse and straw are presented in Table 2 as the average values obtained at the different heating rates. These estimated values agree with the values presented in the study by Najafi et al. (2023) [10].

The SCB has a higher content of holocellulose (cellulose + hemicellulose) when compared to SCS, as observed in Table 2, this result may explain the higher thermal degradation rate observed in SCB, as evidenced in Fig. 1, since a higher amount of polysaccharides in the biomass can result in a highest thermal degradation rate and greater release of volatiles [39]. On the other hand, the lignin content was

Table 2
Results of the compositional analysis of bagasse and straw biomass obtained from the deconvolution of DTG curves.

Component (wt. %)	SCB	SCS	SCB[a]	SCS[a]
Extractives	3.64 ± 0.24	4.06 ± 0.31	6.81 ± 5.24	7.15 ± 4.06
Hemicellulose	32.03 ± 1.17	27.4 ± 0.26	27.87 ± 5.48	28.95 ± 3.25
Cellulose	47.19 ± 0.79	43.68 ± 0.46	40.42 ± 4.76	36.35 ± 3.93
Lignin	17.14 ± 0.51	24.86 ± 0.16	20.14 ± 4.97	24.41 ± 4.54

[a] Average values reported by Najafi et al. (2023) [10].

significantly higher in SCS (24.86 %) compared to SCB (17.14 %). This is in line with the results discussed in the proximate analysis of the biomass, where a higher fixed carbon content indicates a greater lignin content in the material, further corroborating with the highest percentage of final residue in the TGA analysis of sugarcane straw.

3.3. Kinetic and thermodynamic analysis

As observed in the TGA/DTG results of sugarcane bagasse and straw biomasses, the thermal degradation of the constituents of the matrices analyzed mainly occurs during the active pyrolysis phase between 150 and 700 °C, thus, this temperature range was selected for conducting kinetic studies. Fig. 2 illustrates the behavior of the conversion degree, or rate, as a function of temperature according to the analyses at 10, 15, 20, and 25 °C min ^{1} of both biomass samples.

Evaluating the heating rate (β) influence, it was observed that as the value of β increased, the conversion curve experienced a slight shift towards higher temperatures. However, the thermal conversion profile, which is related to the reaction mechanism, remained unchanged, suggesting that the heating rate exerted a low influence on the reaction mechanisms occurring in the thermal degradation process of both analyzed biomasses. Nonetheless, it was observed a greater influence on the conversion rates, which may be attributed to increased heat transfer within the biomass particle, promoting an increase in the conversion ratios under higher heating rates [61,62].

For kinetic modeling, the isoconversional models FWO, KAS, and STK were employed. The conversion range between 0.20 and 0.80 was considered to determine the apparent activation energy (Ea) of the thermal degradation process. The results obtained from the kinetic analysis (linear fitting curves and distribution of Ea values) are shown in Fig. 3.

It was observed in Fig. 3-**A** that all kinetic models used fitted well to the experimental data, showing regressions with high linearity and R^2 values above 0.985, indicating suitability for modeling the kinetics of both sugarcane bagasse and straw pyrolysis. Regarding the Ea values obtained for each sample (Fig. 3-**B**), it was observed that there were no significant differences between the FWO, KAS, and STK methods, indicating high reliability in the modeling using all three methods.

The Ea values of the thermal conversion process of SCB increased from 125 to 160 kJ mol ^{1}, according to the conversion degree increase. The behavior of activation energy in this process can be sequenced into three steps, indicating the occurrence of simultaneous and parallel reactions. In the first steps of the process (α = 0.2–0.5), an increasing trend in Ea was observed with the degree of conversion, from ~ 125 kJ mol ^{1}

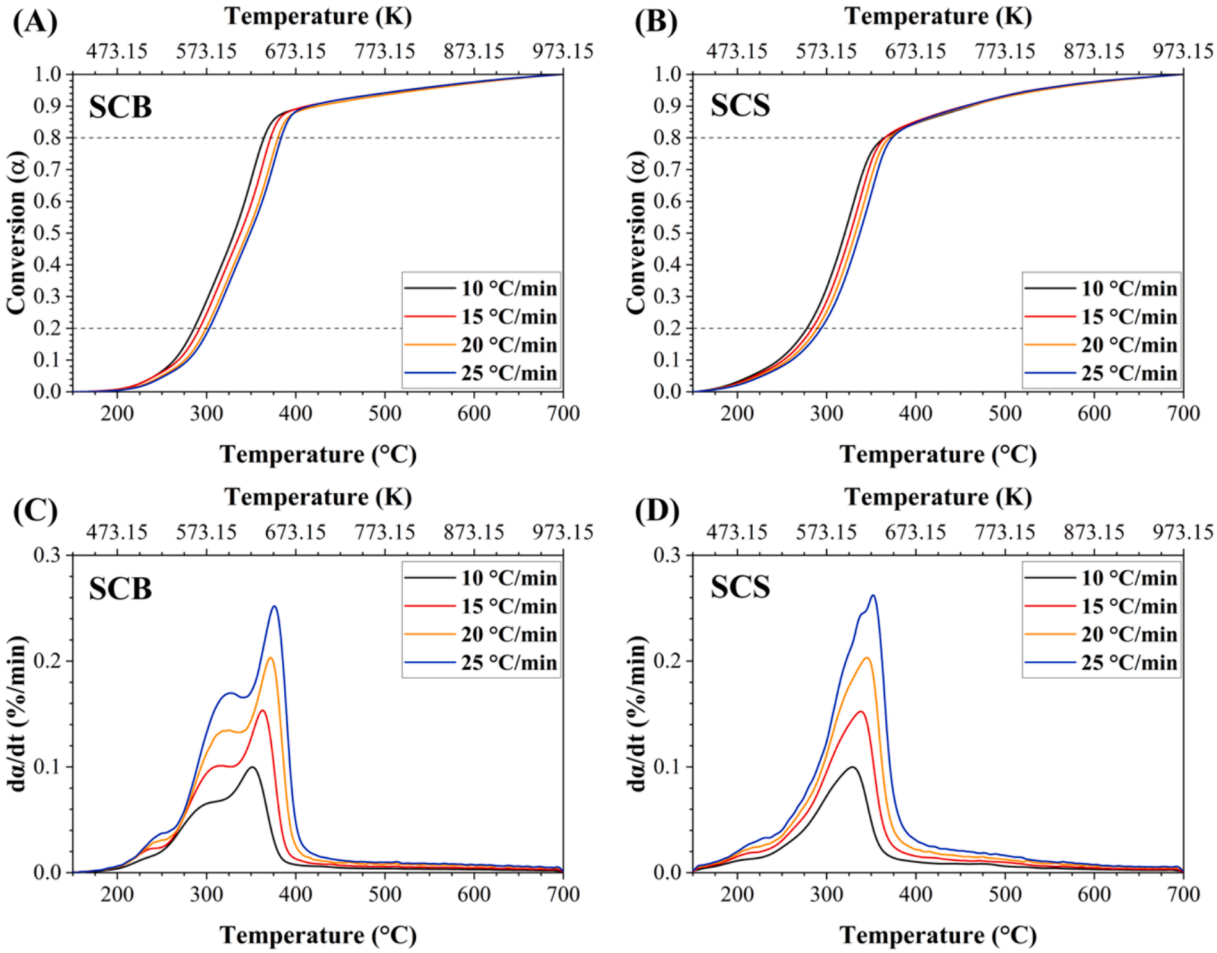

Fig. 2. Thermal conversion curves and their derivatives for the decomposition processes of SCB and SCS at different heating rates.

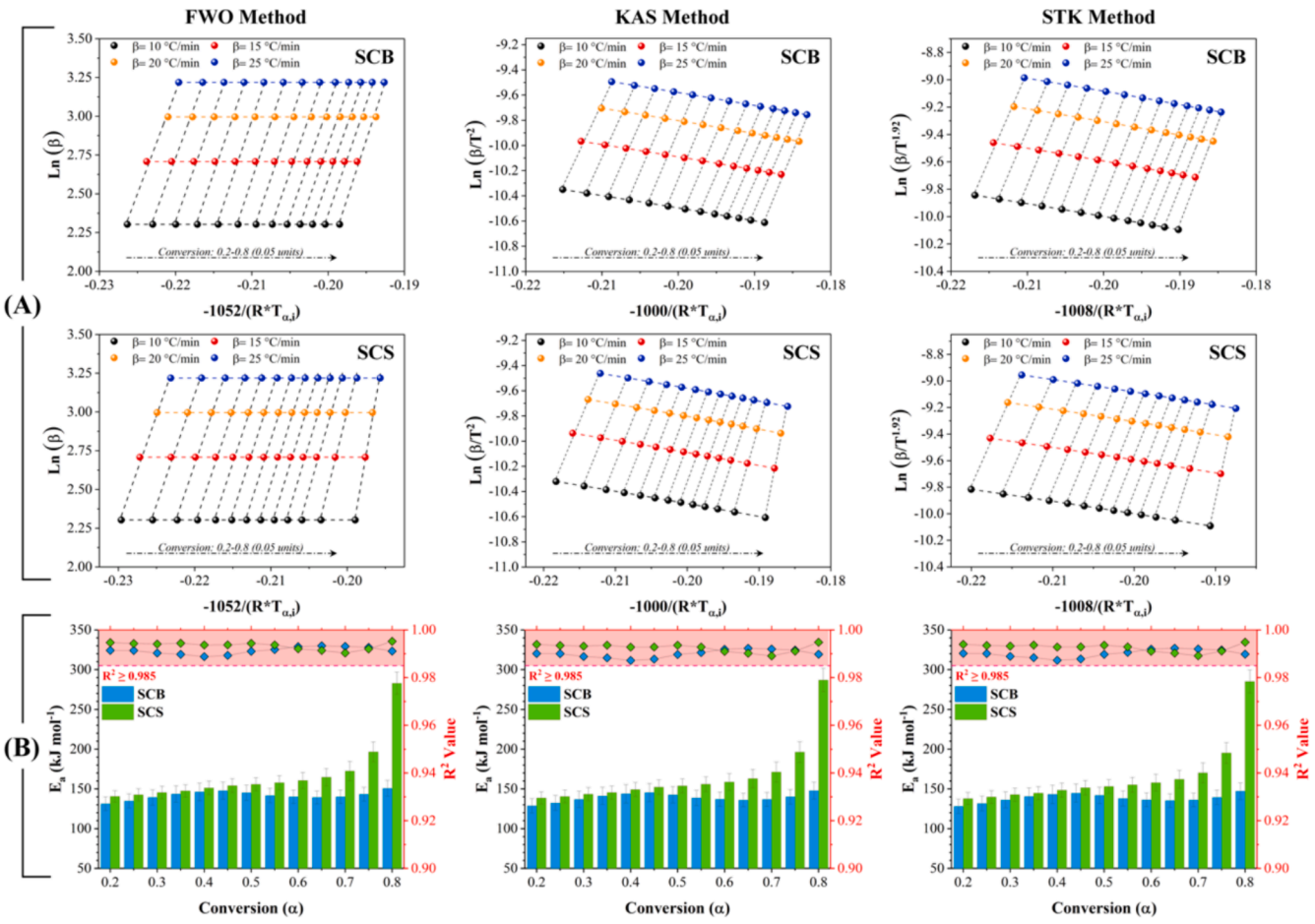

Fig. 3. Kinetic modeling of the thermal degradation of sugarcane bagasse and straw: (A) linear fit curves for the three models evaluated and (B) comparison between the activation energies involved in the thermal conversion process of SCB and SCS.

at α = 0.20 to ~ 150 kJ mol ^{1} at α = 0.5. When correlating the behavior of Ea with the thermal conversion curves of each lignocellulosic constituent of bagasse (Figure S2), it was found that the first steps of the process was mainly related to the cracking of hemicellulose. The tendency for Ea to increase in the hemicellulose degradation process is due to the nature of its more branched polysaccharide structure, with fewer free hydroxyl groups, that during the cleavage process it can induce the formation of more stable structures through condensation reactions, thus requiring greater energy to convert them into molecules with a lower molecular mass [15,60]. When α increased to 0.7, the reactions occurring in the process were mainly related to the thermal degradation of cellulose. At this stage, the activation energy of the process decreased to ~ 140 kJ mol ^{1}. During the cracking of the cellulose structure, it is described that the polymer absorbs energy to reach an intermediate stage called active cellulose (point of highest activation energy), after this point, the fission of active cellulose occurs faster (higher degradation rates), and requiring lower energy rates [60,63,64]. With α values > 0.7, the breakdown of the lignin structure had a greater influence on pyrolysis. Ea values increased as the decomposition process progressed, indicating the formation of thermally stable structures derived from the random condensation of radicals generated by the cleavage of lignin's β-aryl ether bond [65,66].

In the SCS sample, the activation energies involved in the thermal cracking process concentrated in the range from 140 to 290 kJ mol ^{1}. As the degree of conversion increased from 0.2 to 0.5, corresponding to the region mainly associated with the cleavage of the biomass polysaccharide matrix structures, there was an increase in the Ea of the process, from ~ 140 to ~ 155 kJ mol ^{1}. However, as α increased to 0.8, an exponential increase in Ea values was observed, reaching the maximum value of ~ 290 kJ mol ^{1}. This result may be related to the higher lignin content in the straw, which tends to promote greater formation of stable carbonaceous structures during the thermal decomposition process [66,67]. Analyzing the distribution of Ea as a function of the values of α and correlating it with the conversion curves of the lignocellulosic constituents of the straw (Figure S2), it was observed that in this sample, due to the higher lignin content, this polymer exerted a greater influence throughout the conversion range studied, also affecting the decomposition reactions of the other lignocellulosic components, which suggests the occurrence of simultaneous and combined reactions between the intermediates derived from each constituent of the biomass. This interaction between intermediates from the polysaccharide matrix and lignin derivatives contributed to greater complexity in the pyrolysis of straw, in line with the increase in Ea as the thermal conversion process progressed [68]. Additionally, the higher ash content in the straw may have contributed to the higher Ea values in SCS pyrolysis, as ashes tend to limit the heat and mass transfer process, hindering the thermal cracking process [69].

The average values of Ea for the SCB sample were 141.17 kJ mol ^{1}, 139.02 kJ mol ^{1}, and 138.32 kJ mol ^{1} for the FWO, KAS, and STK methods, respectively. For the SCS sample, the average values were 167.06 kJ mol ^{1}, 165.76 kJ mol ^{1}, and 164.85 kJ mol ^{1} for the three models used, respectively. Considering that the Ea represents the minimum amount of energy that must be supplied to the system to overcome the energy barrier and favor the formation of products in a chemical reaction [70], the higher average Ea values for the SCS biomass suggest that, compared to SCB, the straw has a more recalcitrant and stable

structural formation, requiring higher energy rates to promote the occurrence of molecular rearrangements that induce the formation of active intermediates and consequently the formation of pyrolytic products [47,69].

For conducting the thermodynamic analysis of the thermal conversion processes, it was decided to use only the Ea obtained by the Starink model, since the variations between the Ea obtained by different kinetic models were not significant, moreover, among the models used it is considered more accurate by the Kinetics Committee of the International Confederation for Thermal Analysis and Calorimetry (ICTAC) [71]. Furthermore, the slowest heating rate was chosen to facilitate the identification of possible changes in data behavior as the degree of conversion progresses. Thus, the thermodynamic parameters were calculated using the data from the analysis conducted under the heating rate of 10 °C min ^{1}. The pre-exponential factors and thermodynamic parameters involved in the thermal conversion of bagasse and sugarcane straw are available in Table 3.

The pre-exponential factors (A) involved in the studied processes varied from 10^{10} to 10^{11} min ^{1} for the SCB thermal degradation and 10^{11} to 10^{24} min ^{1} for SCS, at the conversion range from 0.2 to 0.8. The variation trend of A with increasing conversion resembles the variation observed in the activation energy, as shown in Fig. 3-**B**, indicating an increase in the complexity of reactions as the process advances [66]. This suggests the presence of multiple reactions in pyrolysis, especially for the SCS sample, which varied over a wider range. The smaller variation of A in the bagasse conversion process, compared to straw, suggests a greater uniformity in the SCB cracking reactions, which may be related to its more abundant composition in cellulose and hemicellulose. Furthermore, all values found exceed the order of 10^{10} min ^{1}, indicating a higher frequency of intermolecular collisions, promoting the occurrence of complex reactions, not limited only to surface mechanisms [72].

Upon analyzing the enthalpy variation (ΔH*), it is noted that during the pyrolysis of SCB, the values concentrated in the range of 123 to 142 kJ mol ^{1}, with an average value of 133.32 kJ mol ^{1}. However, in the thermal cracking process of SCS, ΔH* values ranging from 133 to 280 kJ mol ^{1} was observed, with an average value of 159.92 kJ mol ^{1}. These values with positive signals are in line with the endothermic nature of the pyrolysis process [73]. Additionally, considering that ΔH* represents the energy required to decompose biomass into volatile compounds and char, the higher ΔH* values in SCS pyrolysis, indicate that the straw decomposition process demands higher energy consumption for the production of pyrolytic products than in SCB pyrolysis [74]. The difference between the values of Ea and ΔH* oscillated from 4.5 to 5.5 kJ mol ^{1} for both biomasses, reflecting a low potential energy barrier, suggesting that the formation of the activated state is favorable, making the pyrolysis process viable [75].

Regarding entropy, a state function used to analyze the degree of disorder and randomness of a reactional system, it was observed negative values of entropy variation (ΔS*) on the thermal conversion process of SCB across the entire range of evaluated conversion, ranging from –95.09 to –64.57 J mol ^{1} K ^{1}. This indicates a more ordered system closer to thermodynamic equilibrium [76]. In contrast, in the SCS pyrolysis, ΔS* oscillated between negative and positive values, showing a tendency to increase ΔS* with the value of α. For the SCS sample, the entropy variation increased from –69.94 to –15.33 J mol ^{1} K ^{1} as α rose from 0.2 to 0.7. At conversions greater than 0.7, ΔS* became positive, reaching the maximum value (179.65 J mol ^{1} K ^{1}) at α = 0.8. This indicates that the straw pyrolysis reaction system becomes more reactive as the conversion progresses, deviating from thermodynamic equilibrium towards the end of the process, which is characteristic of a more complex reactional system [77,78].

The recoverable energy potential of biomass through the pyrolysis process can be assessed by the variation of Gibbs energy (ΔG*) [53]. The ΔG* values involved in the pyrolysis of SCB ranged from 176 to 183 kJ mol ^{1}, with an average value of 180.51 kJ mol ^{1}. In the conversion of SCS, ΔG varied between 165 and 175 kJ mol ^{1}, with an average value of 173.13 kJ mol ^{1}. The ΔG positive values confirm the non-spontaneity of the pyrolysis process, as energy input is required to promote the thermal cracking reactions. Furthermore, the higher ΔG values obtained in the SCB sample suggest a greater energy potential for conversion into products through pyrolysis [79].

Table 3
Pre-exponential factors and thermodynamic parameters involved in the thermal conversion of sugarcane bagasse and straw using the 10 °C min^{-1} heating rate.

Conversion (α)	A (min ^{1})	ΔH* (kJ mol ^{1})	Ea-ΔH* [a] (kJ mol ^{1})	ΔS* (J mol^{-1}K ^{1})	ΔG* (kJ mol ^{1})
Sugarcane bagasse pyrolysis					
0.20	2.05×10^{10}	123.42	4.65	–95.09	176.57
0.25	4.19×10^{10}	126.91	4.72	–89.27	177.56
0.30	1.03×10^{11}	131.33	4.78	–81.92	178.45
0.35	2.45×10^{11}	135.62	4.84	–74.80	179.20
0.40	4.19×10^{11}	138.25	4.91	–70.44	179.81
0.45	5.69×10^{11}	139.72	4.97	–68.00	180.34
0.50	3.25×10^{11}	136.85	5.02	–72.77	180.81
0.55	1.49×10^{11}	132.89	5.07	–79.33	181.31
0.60	1.06×10^{11}	131.14	5.12	–82.24	181.81
0.65	8.78×10^{10}	130.16	5.17	–83.87	182.27
0.70	1.03×10^{11}	130.91	5.21	–82.62	182.65
0.75	1.97×10^{11}	134.11	5.25	–77.30	182.92
0.80	9.18×10^{11}	141.78	5.30	–64.57	182.94
Sugarcane Straw pyrolysis					
0.20	4.16×10^{11}	133.22	4.58	–69.94	171.76
0.25	6.19×10^{11}	135.05	4.66	–66.79	172.52
0.30	1.13×10^{12}	137.88	4.73	–61.92	173.13
0.35	1.72×10^{12}	139.86	4.79	–58.52	173.58
0.40	3.74×10^{12}	143.57	4.84	–52.14	173.94
0.45	6.92×10^{12}	146.50	4.89	–47.11	174.21
0.50	9.64×10^{12}	148.07	4.93	–44.43	174.44
0.55	1.48×10^{13}	150.10	4.98	–40.94	174.61
0.60	2.60×10^{13}	152.78	5.02	–36.34	174.72
0.65	6.23×10^{13}	156.99	5.06	–29.13	174.73
0.70	3.31×10^{14}	165.05	5.11	–15.33	174.47
0.75	5.64×10^{16}	190.03	5.17	27.31	173.04
0.80	5.23×10^{24}	279.82	5.29	179.65	165.57

[a] Potential energy barrier; *Transitional state.

3.4. Distribution of pyrolysis products and characteristics of biochar

To enhance the assessment of the sugarcane residues' thermal conversion process to produce renewable chemical inputs, the studied biomasses underwent microscale pyrolysis experiments at 500 °C. The yields of the resulting products and the compositional characteristics of

the pyrolytic gas and the biochar are presented in Table 4.

It was observed in Table 4 that the total liquid fraction (aqueous fraction + bio-oil) was the main pyrolysis product for both sugarcane bagasse and straw. The yield of this product was slightly higher for the SCB sample (~63 %) compared to the SCS sample (~58 %). The liquid products consist predominantly of LMM fraction, accounting for approximately 62 % yield for SCB and 55 % for SCS pyrolysis. Due the condensation temperatures, it is suggested that the LMM corresponds to a mixture rich in monomeric organic compounds, as well as water derived from biomasses dehydration during the pyrolysis process. On the other hand, the HMM fraction represents a mixture rich in polar oligomers derived from the cracking of lignocellulosic constituents, mainly phenolic oligomers from lignin (pyrolytic lignin) and products of condensation reactions between unstable intermediates derived from the cracking of the lignocellulosic components of biomass [80–82]. The production of HMM was higher in the pyrolysis of SCS (3.4 %) compared to SCB (1.7 %), which may be related to the higher lignin content in straw, leading to a greater production of pyrolytic lignin. In addition, the higher production of HMM in the SCS is in line with the results of the kinetic analysis, where it was proposed that in the pyrolysis of straw there is a greater interaction of lignin derivatives with holocellulose derivatives resulting in the formation of stable structures (compounds present in the high molecular mass fraction) and leading to an increase in the activation energy of the process. Regarding the gaseous product, it was observed that the SCB pyrolysis yielded ~16 % of gases, while SCS thermal conversion yielded ~8 % of pyrolytic gas. Correlating these results with the biomasses characteristics detailed in Table 1 and 2, it is noted that the higher yield of gases and liquids products in the thermal conversion of SCB may be related to the greater content of volatile material and holocellulose (hemicellulose + cellulose) present in this biomass [83].

About the pyrolysis solid product, a higher biochar yield was observed in the SCS pyrolysis, reaching ~33 % of biochar, while the conversion of SCB resulted in ~20 % of this product. The higher solid production in straw pyrolysis is associated with the high ash content as well as the higher lignin content, which is a significant component in the formation of carbonaceous structures [54,84]. This result was consistent with the observations discussed in the thermogravimetric and kinetic analysis section, revealing that straw, compared to bagasse, due to the greater reaction interaction between the unstable derivatives of the lignocellulosic constituents, induces the production of more thermally stable carbonaceous structures. The produced biochars were mainly composed of carbon (C) and oxygen (O), with 68.41 % of C and 11.73 % of O observed in the SCB biochar and a content of 59.28 % C and 11.48 % O in the SCS biochar. Higher values of molar ratios H/C, O/C, and N/C were observed for straw-derived biochar compared to the produced from bagasse. This result suggests that SCS biochar has a more functionalized structure, as well as a higher mineral content due to the high ash content (~25 %) [85]. Bagasse biochar, on the other hand, presents a structure with a higher degree of condensation, as evidenced by the lower value of the H/C ratio, and has a higher energy content due to greater carbon content [86]. These results indicate that the obtained products may have distinct applications in the industrial sector. For example, straw-derived biochar, due to its higher degree of functionalization and higher mineral content, shows potential to be used as a soil enhancement agent in sugarcane cultivation or in applications as a pollutant adsorbent, which can be used in effluent treatment or CO_2 adsorption [87–89]. Meanwhile, bagasse-derived biochar can be directed toward energy purposes in the sugarcane industry or as energy storage devices [14,90].

Table 4
Gravimetric yields of the pyrolytic products and composition of the biochar obtained from the pyrolysis of sugarcane bagasse and straw.

Product	SCB	SCS
Gravimetric yields (% wt.)		
Sum of Liquid Product	63.51 ± 1.93	58.03 ± 1.05
Low Molecular Mass Fraction (LMM)[a]	61.83 ± 1.57	54.65 ± 0.54
High Molecular Mass Fraction (HMM)[b]	1.68 ± 0.36	3.38 ± 0.51
Gases	16.15 ± 0.92	8.3 ± 0.90
Biochar	20.34 ± 1.29	33.67 ± 1.10
Biochar Composition (% wt.)		
C	68.41 ± 0.34	59.28 ± 0.44
H	2.61 ± 0.18	3.11 ± 0.11
N	0.86 ± 0.06	1.02 ± 0.05
O[c]	11.73 ± 0.56	11.48 ± 0.46
Ash[d]	16.4 ± 0.75	25.36 ± 0.53
H/C Molar Ratio	0.458	0.605
O/C Molar Ratio	0.129	0.145
N/C Molar Ratio	0.011	0.015
HHV (MJ Kg ^{1})	26.15	23.39

[a] Liquid fraction rich in non-condensable compounds at 350 °C; [b] Liquid fraction rich in condensable species at 350 °C; [c] Obtained by difference; [d] Estimated based on the biomasses ash contents.

3.5. *Characterization of volatile compounds present in the low molecular mass liquid fraction by GC/MS*

The LMM fractions chromatograms derived from the SCB and SCS pyrolysis revealed a similar compositional profile between them (see Supplementary Material, **Figure S4**). The same chromatographic peaks were observed in both samples, with differences in their intensities. This suggests that concerning the organic fraction analyzable by GC, the liquid products contain the same compounds but with distinct relative concentrations for each chemical species. Approximately 70 to 79 % of the total relative area of the chromatographic peaks was identified, and the compounds were categorized into different chemical classes according to their main organic functions, such as alcohols, carboxylic acids, phenols, and sugar derivatives. The distribution of compounds according to their chemical class is shown in Fig. 4. The list of identified compounds is available in **Table S3**.

The LMMs analysis revealed structures derived from the thermal degradation of the lignocellulosic biopolymers of the biomass. In both samples, the major classes were compounds derived from sugars and phenolic compounds, which together accounted for about 55 % of the total area of the chromatogram. A slightly higher content of sugar derivatives was observed in the liquid product resulting from bagasse pyrolysis. In the SCB-derived sample, the percentage area of this compounds class was approximately 30 %, while in the SCS-derived sample, a relative content of about 25 % was observed. On the other hand, the LMM derived from SCS presented ~30 % of phenolic content, while in the SCB-derived sample this content was about 23 %. The production of sugar derivatives is associated with the cracking of the biomass holocellulose matrix, while the formation of phenolic species derives from

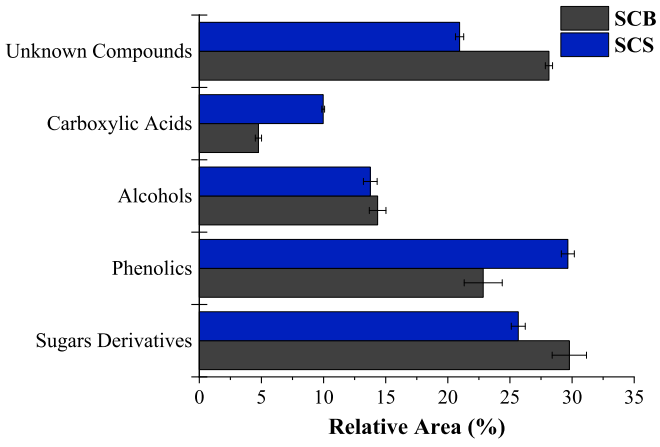

Fig. 4. Histogram of classes obtained from GC/MS analysis of LMMs produced from the pyrolysis of sugarcane bagasse and straw.

the lignin degradation [16,91]. Thus, the results observed in the GC/MS analysis are in accordance with the holocellulose and lignin contents determined for each biomass, where the higher content of polysaccharides in bagasse induced the production of a liquid product with a higher content of sugar derivatives, and the higher lignin content in straw promoted a greater production of phenolic constituents.

In addition to sugar and phenolic derivatives, the production of compounds from the alcohol and carboxylic acid classes derived from the secondary cracking of biomass constituents was also observed [16]. Both biomasses produced pyrolytic liquids with an alcohols content of approximately 14 %, mainly represented by isobutanol and ethylene glycol, while the acid content was ~5 % for the SCB-derived LMM and ~10 % for the SCS-derived sample. The sugarcane residues pyrolysis generated a wide range of chemicals with high added value, such as isobutanol, furfuryl alcohol, 4-hydroxybutanoic acid, 4-vinylphenol, 2-methoxy-5-methylphenol, catechol, 4-vinylguaiacol, D-ribofuranose, 2-deoxy-D-*erythro*-pentopyranose, and levoglucosan, which are of great interest to both the industrial and energy sectors [92]. Thus, the conversion of residual raw materials from sugarcane processing exhibits high potential to produce renewable chemicals and can promote diversification of the product portfolio in the sugarcane industry.

3.6. Characterization of low and high molecular mass liquid fraction by UHRMS analysis

3.6.1. Positive mode analysis using heated electrospray ionization (H-ESI (+)-FT-Orbitrap MS)

Fig. 5 presents the results of the analysis conducted on the diverse liquid product fractions obtained from the SCB and SCS pyrolysis.

The mass spectra and the molecular mass distribution plot revealed that compounds in the LMM and HMM fractions distribute in distinct mass regions. Species present in the LMM fractions derived from both SCB and SCS are predominantly distributed in the *m/z* range from 100 to 400, with the most intense compounds presenting molecular mass less than 250 Da. For the HMM samples, different profiles were observed between the two studied biomass sources. In the SCB-derived HMM fraction, compounds are mainly distributed between *m/z* 150 to 600, with the most intense compounds situated in the molecular mass range of 200 to 500 Da. In contrast, in the SCS sample, species are distributed between *m/z* 100 and 500, with compounds with molecular masses between 150 and 400 Da being the most abundant in the spectrum. The HMM fraction of the SCS bio-oil exhibited a higher intensity of compounds in the 100 to 250 Da range, compared to the sample derived from bagasse at the same *m/z* range. This result suggests that analyzable compounds by H-ESI(+) from straw's HHM exhibit a characteristic of lower molecular weight compared to bagasse's HMM.

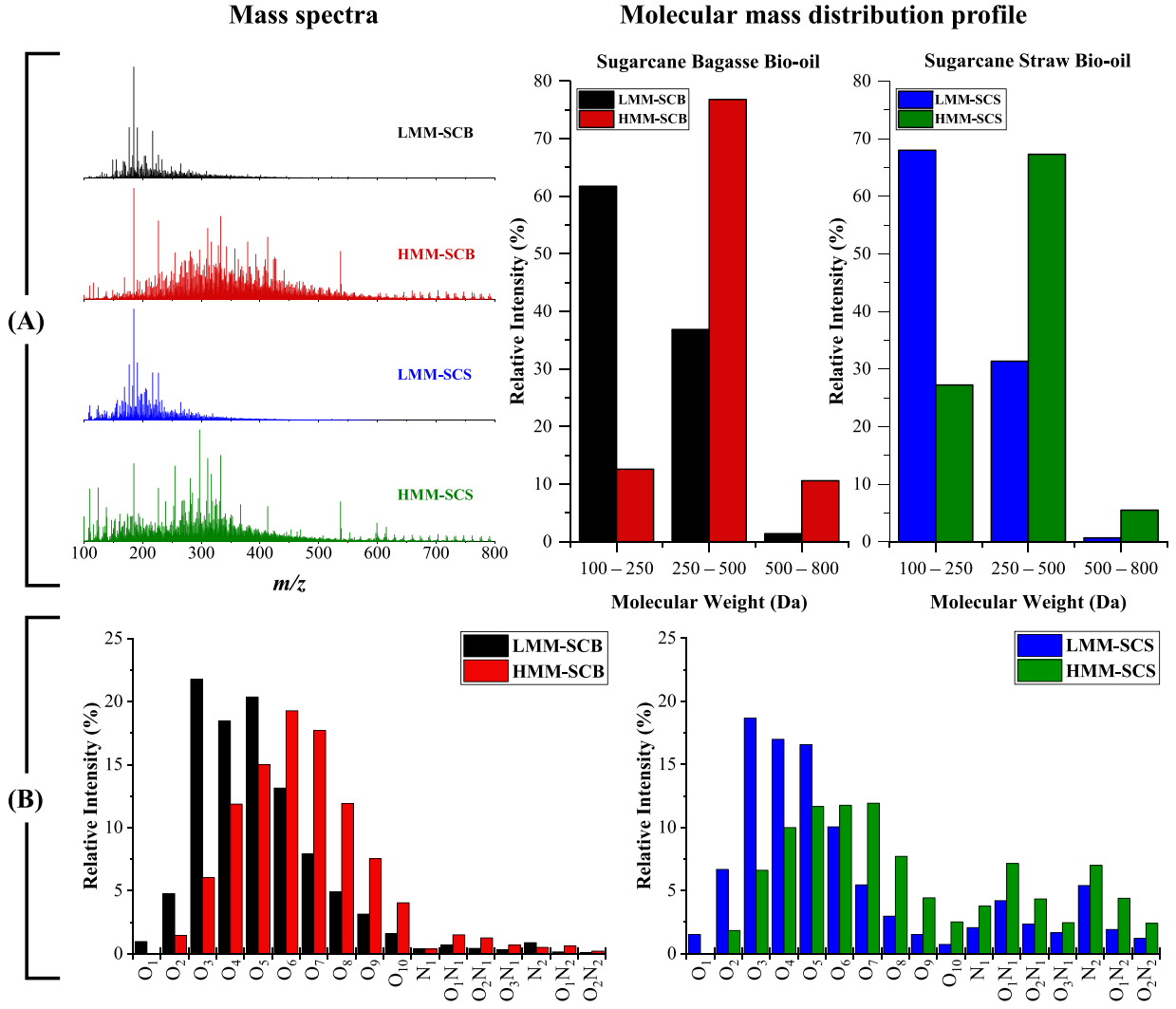

Fig. 5. Mass spectra and molecular mass distribution profile of the compounds present in the pyrolytic liquid fractions analyzed by H-ESI(+) (A) and (B) heteroatom classes histograms.

In the H-ESI(+) analysis of the LMM and HMM fractions was detected about 3805 to 4890 ions, with approximately 1863 to 2400 molecular formula assignments, corresponding to between 41 and 55 % of the detected ions in the samples Fig. 5**-B**, LMM and HMM samples presented the same chemical classes except for O_1 which was absent in HMM. The oxygenated species were distributed into $O_{1–10}$ classes, and nitrogen-containing compounds were distributed into $N_{1–2}$ and $O_{1–3}N_{1–2}$ classes according to the assigned molecular formula.

Regarding the class distribution profile as a function of relative intensity, it was observed that both LMM samples exhibited higher intensity for compounds in $O_{1–5}$ classes. In contrast, HMM samples displayed higher intensity for $O_{6–10}$ classes. Additionally, the relative intensity of the nitrogen-containing classes was greater in the HMMs oils, suggesting that nitrogenous constituents formed in the pyrolysis of the studied biomass have higher thermal stability and tend to remain in the heavy fraction of the bio-oil. The higher intensity observed for the $O_{6–10}$ classes, indicates that the obtained HMM fractions possess a higher degree of functionalization or a greater content of phenolic oligomeric species.

Comparing the SCB and SCS bio-oils, a higher intensity was observed

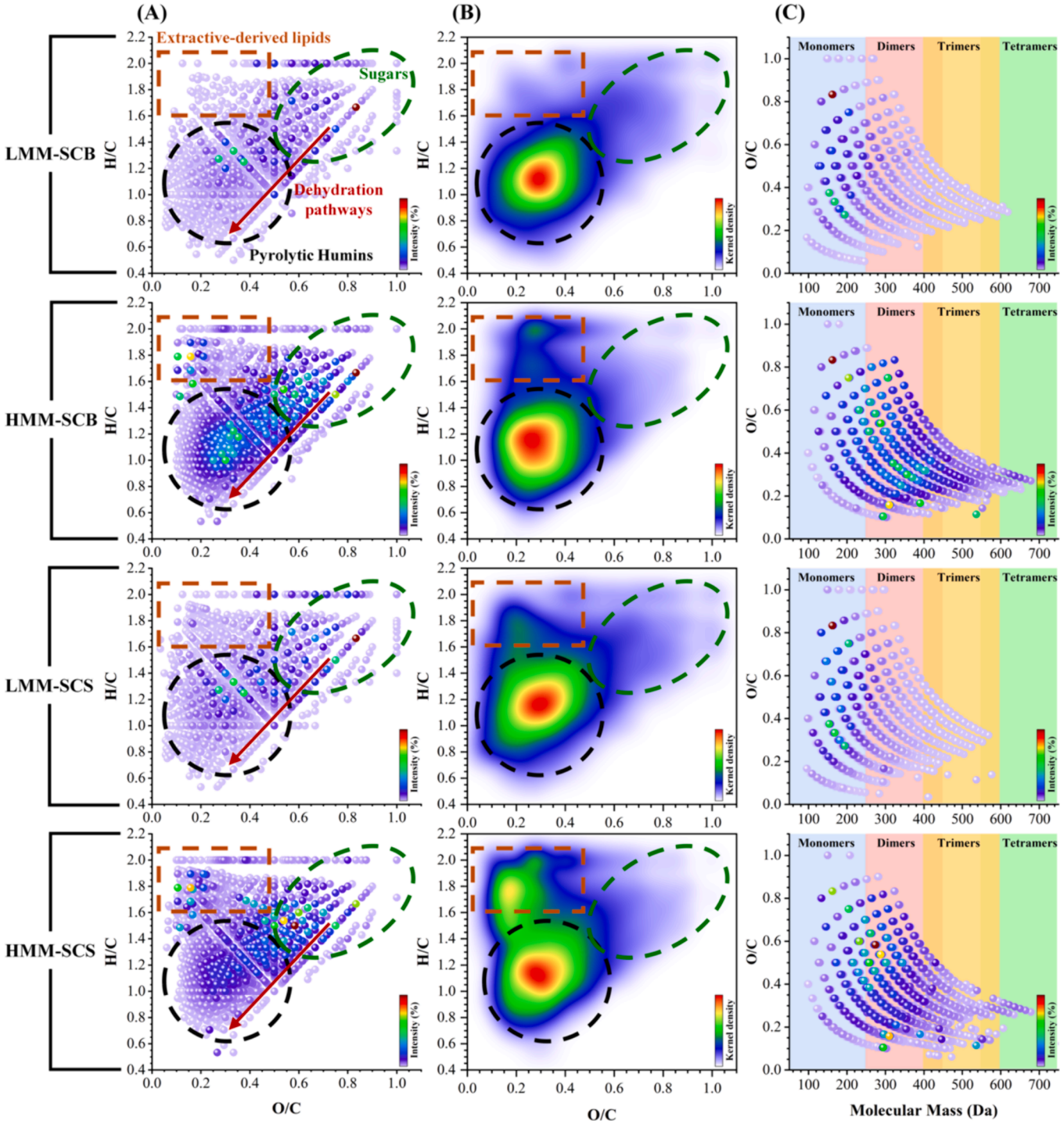

Fig. 6. H/C vs O/C ratio van Krevelen diagrams as a function of relative intensity (A) and molecular population density (B). Plots of O/C vs molecular mass of the pyrolytic oxygenated compounds (C).

for oxygenated compounds in the samples derived from the SCB pyrolysis, which summed up to approximately 97 % and 94 % for the LMM and HMM samples, respectively. For the samples derived from SCS conversion, the total intensity of oxygenated classes was about 81 % for LMM and 68 % for HMM. However, the fractions derived from SCS showed higher intensities for nitrogenated classes, approximately 19 % and 32 % for LMM and HMM, respectively. In SCB-derived samples, the sum of the intensity of nitrogenated constituents was approximately 3 % and 5 % for LMM and HMM, respectively. Considering that the formation of nitrogenated species during the pyrolysis of lignocellulosic biomass derives from the protein matrix present in the feedstock [93], these results indicate a higher availability of proteins in biomass derived from sugarcane straw [10,94]. It is also important to consider that basic nitrogenated species generally exhibit high ionization efficiency in the H-ESI source, causing these compounds to produce ions with high intensities in mass spectra, which cannot be directly correlated with their concentration in the sample [95,96]. Further, the low nitrogen content present in the studied biomass (<0.5 %), a low concentration of nitrogenated species is expected compared to oxygenated ones in the lignocellulosic bio-oils.

To achieve a more detailed bio-oil molecular characterization, van Krevelen diagrams are widely used, which are elaborated based on the atomic ratios (H/C vs O/C, N/C, or S/C) as a function of the relative intensity of the compounds or as a function of the molecular population density, that is estimated through Kernel density. By correlating the atomic ratios, it is possible to identify possible reaction pathways between different processes, as well as to perform speciation of the compound's base structures. This allows describing which kind of compounds predominate in the sample under study [97]. Furthermore, atomic ratio vs molecular mass plots have recently been used to favor better speciation between monomeric and oligomeric species [98,99]. In this way, the molecular distribution of the compound classes containing only oxygen was evaluated in the van Krevelen diagram of H/C vs O/C atomic ratio and the O/C vs molecular mass diagram, as shown Fig. 6.

The oxygenated species present in the samples are distributed in a H/C range varying between 0.5 and 2.0 and an O/C ratio between 0.1 and 1.0 as observed in Fig. 6-**A**. The LMM samples from both studied biomasses exhibited a similar pattern of molecular distribution. Regarding the HMM fractions, a similar compound distribution was observed, although relative intensity variations in signal molecules have been seen. These results indicate that the oxygenated species produced during pyrolysis exhibit similar characteristics to each other, and differ only in the quantity formed, regardless of the biomass used. The oxygenated compounds are in three main regions in the van Krevelen diagrams, which can be correlated to specific molecular characteristics for the compound classes, making it possible to identify the base structure (skeleton) of the compounds. The region with H/C between 1.6 and 2.0 and O/C < 0.4 is typically attributed to lipid derivatives, due to its aliphatic characteristics and low O/C ratio [24]. Species grouped in the region of H/C ranging from 1.2 to 2.0 and O/C > 0.5 are characteristic of predominantly naphthenic and/or aliphatic structures, with a high O/C ratio, which may be related to molecules derived from sugars, produced by the thermal degradation of the holocellulose matrix of the biomass [100]. In the region localized at O/C 0.02 – 0.6 and H/C 0.6 – 1.5 in Fig. 6-**A**, a high density of molecules with H/C between 1.0 and 1.3, characteristics of aromatic molecules, and with an O/C ratio < 0.5 was observed, which could be attributed to a fraction of highly dehydrated holocellulose derivatives rich in furanic rings, called pyrolytic humins [101].

In the van Krevelen diagrams as a function of molecular population density (Fig. 6-**B**), it was observed that the identified species predominantly cluster in the region attributed to pyrolytic humins structures. This result suggests that during pyrolysis, structures derived from the primary cracking of the biomass polysaccharide matrix underwent secondary dehydration and condensation reactions, thus promoting the formation of a high number of condensed furanic species [22,102]. Comparing the two produced LMM fractions, it was observed that the region of lipid-derived compounds showed a higher population density in the SCS sample. This behavior was also observed in the HMM fractions, suggesting a greater abundance of lipid constituents in the extractive fraction of the straw biomass. Regarding sugars (highlighted region in green in Fig. 6-**B**), higher densities were observed for the LMM samples compared to the HMMs, suggesting that the compounds located in this region correspond mostly to monomeric species, as detected in the GC/MS analysis.

From the O/C vs molecular mass graphs in Fig. 6-**C**, it was observed that the oxygenated compounds analyzable by H-ESI(+) from the SCB and SCS bio-oil fractions were distributed along trend lines. Each trend line corresponds to an oxygenated compound class, which, from left to right, refers to the O_1 to O_{10} classes in the LMM fractions and O_2 to O_{10} in the HMM samples. The compounds present in the LMM fractions are distributed in the mass range from 50 to 600 Da, while the oxygenated species in the HMM fractions are distributed from 100 to 750 Da. According to the mass range compounds distribution, they were classified into monomers (100 to 250 Da), dimers (250 to 450 Da), trimers (400 to 600 Da), and tetramers (550 to 750 Da) [103].

It was observed that the oxygenated compounds were distributed similarly in the O/C vs the molecular mass plots in the LMM fractions from the SCB and SCS pyrolysis. The species with higher intensity in the low molecular mass samples corresponded to molecules from O_3 to O_5 classes, which is consistent with the observed in the class histograms in Fig. 5. However, through Fig. 6-**C**, it was possible to identify that these compounds mainly correspond to monomeric sugar structures, corroborating observation in the van Krevelen diagrams. The compounds from $O_{6–10}$ classes, on the other hand, corresponded to dimer and trimer structures, and due to present predominantly O/C ratios between 0.2 and 0.6, they were attributed to oligomers of the pyrolytic humins fraction [101,104]. Regarding the HMM fractions, a higher degree of polymerization was observed, where species from O_3 to O_8 classes with dimer and trimer structural characteristics were the most intense. In the HMM derived from SCB conversion, a higher abundance of compounds in the trimer and tetramer regions was observed. This result is consistent with the molecular mass distribution profiles presented in Fig. 5-**A**, where higher intensities were observed for species with molecular masses between 250–800 Da in the HMM-SCB sample compared to HMM-SCS.

Regarding nitrogen-containing classes, the molecular characteristics of these compounds were analyzed using DBE (double bond equivalent) vs Carbon Number diagrams, allowing for the analysis of molecules according to the degree of aromaticity and size of the carbonaceous skeleton. These plots are available in the supplementary materials, **Figure S4**. The SCB and SCS LMM samples are composed by nitrogenous species containing between 5 and 25 carbon atoms per structure and a DBE value ranging from 4 to 15 (aromatic structures). The HMM samples, on the other hand, exhibit compounds with a higher degree of aromaticity and carbon chain compared to the LMM fractions. This result is more noticeable in the N_1 class, where in the HMM samples, a region of compounds with a carbon number ranging from 20 to 45 and DBE<10 was observed. In all samples, there is a predominance of species with DBE > 4, suggesting that the nitrogenated constituents of the bio-oils correspond mainly to unsaturated and/or aromatic structures, with carbonaceous skeletons containing, for example, pyridinic rings in their composition (DBE 4) or pyrrole structures (DBE 3) with other oxygenated functional groups [26,93].

Comparing the SCB and SCS bio-oils, it was observed that the samples derived from straw, compared to bagasse, showed a higher number of compounds in all nitrogen-containing classes. However, the distribution pattern of molecules according to the DBE and the carbon number shows similar trends between the LMMs and HMMs fractions produced by both SCB and SCS. This suggests that, although the pyrolysis of straw results in a greater number of nitrogenous components, the protein matrix of both biomasses presents similar compositional

characteristics, tending to produce nitrogenous species with equivalent molecular properties [93].

3.6.2. *Negative mode analysis using atmospheric pressure chemical ionization (APCI (–)-FT-Orbitrap MS)*

The analysis results for speciation of acidic components and phenolic derivatives in bio-oil fractions using APCI(–) are shown in Fig. 7.

Different molecular distribution profiles were observed between the LMM and HMM fractions of the bio-oils (Fig. 7**–A**. Compounds detected in the LMM samples from both studied biomasses were mainly distributed in the *m/z* range from 100 to 500, with species presenting molecular masses between 100 and 250 Da being the most abundant. Regarding the compounds present in the HMM fractions, the mass spectra of the HMM-SCB and HMM-SCS samples revealed that molecules were predominantly distributed in the *m/z* range between 100 and 600, with the most intense compounds restricted to the molecular mass range from 250 to 500 Da. Comparing the two biomasses, the profiles observed for the LMM and HMM fractions derived from SCB and SCS are similar, suggesting that acidic compounds produced from these two feedstocks present similar characteristics.

The analysis of samples in negative mode resulted in the detection of between 3365 and 4752 ions, with a total assignment or molecular formulas ranging from 1344 to 1987, which corresponds to a characterization percentage from 37 to 48 % of the detected ions in the SCB and SCS samples. The identified species were grouped into class histograms (Fig. 7**–B**), where only the presence of oxygenated compounds containing 1 to 10 oxygen atoms per structure was observed in all samples. Besides LMM samples presenting a lower range of molecular mass distribution compared to the HMMs, it also showed higher intensity for the less oxygenated classes (O_1 to O_4). In the HMM fractions were observed higher relative abundances for the compound classes containing from 5 to 10 oxygen atoms per structure, which is consistent with the higher degree of functionalization and/or oligomerization present in the heavy fractions of the bio-oils. Comparing the two feedstocks, differences were observed only in the intensities of the identified classes, especially for compounds in class O_2, which were more intense in the samples produced from straw, suggesting, for example, a higher intensity of carboxylic acids in these samples, mainly fatty acids derived from the cracking of lipids present in the matrix. To confirm this information, the van Krevelen diagrams as a function of relative intensity and molecular population density, as well as the O/C ratio vs molecular mass graphs, are presented in Fig. 8.

In Fig. 8-**A**, it was observed that the species detected in the LMM and HMM samples through APCI(–) analysis are distributed in the van Krevelen diagram within a H/C range from 0.4 to 2.0 and O/C lower than 1.0. Despite using different biomass, the molecular distribution profiles of the species in the LMM and HMM samples are similar, with the greatest differences noted in the relative intensity of the compounds. This result is in agreement with that was observed in the analysis by H-ESI(+) and indicates that the acidic constituents of the SCB and SCS bio-

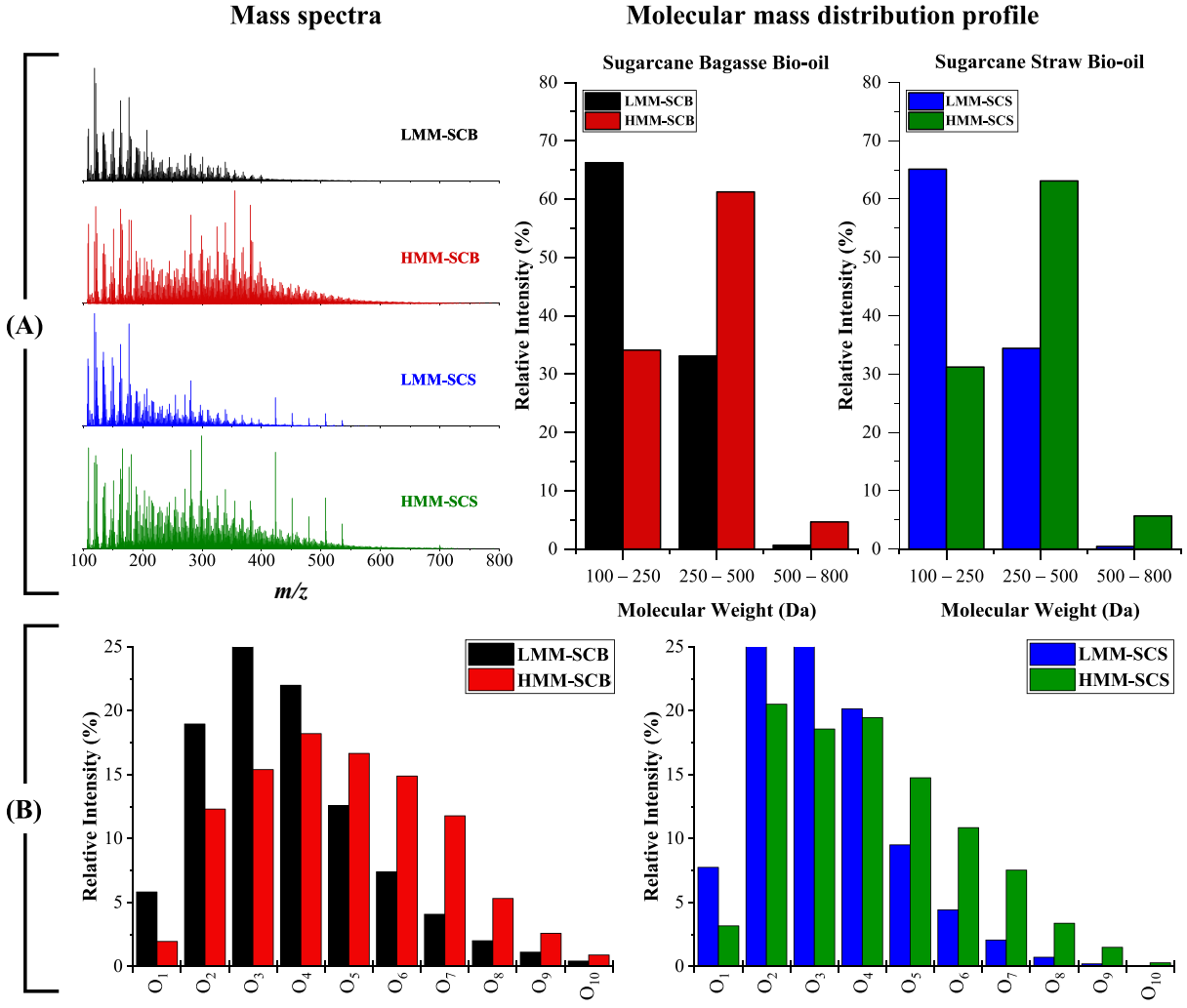

Fig. 7. Mass spectra and molecular mass distribution profile of the compounds present in the pyrolytic liquid fractions analyzed by APCI(–) (A) and (B) heteroatom classes histograms.

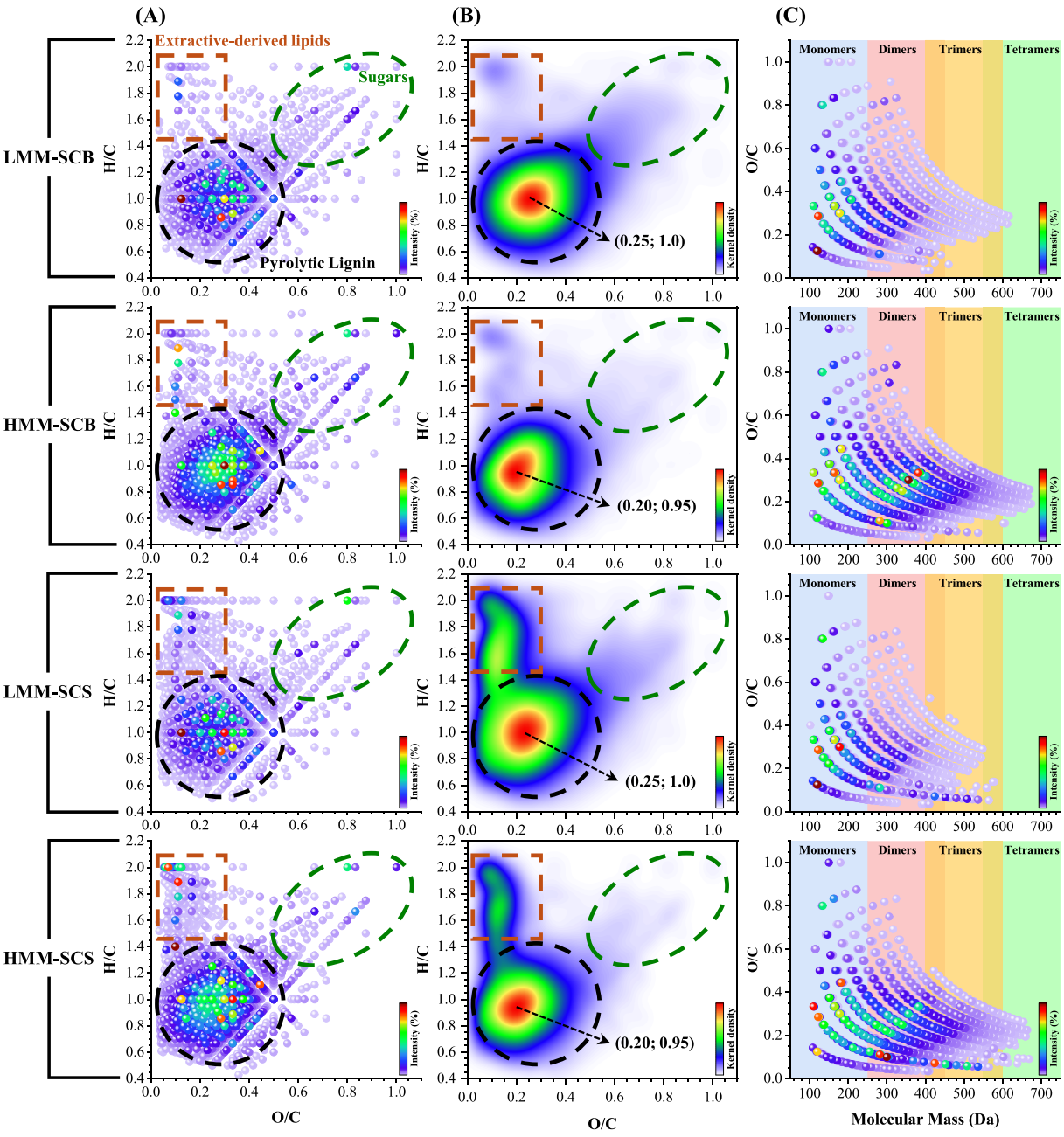

Fig. 8. H/C vs O/C ratio van Krevelen diagrams as a function of relative intensity (A) and molecular population density (B). Plots of O/C vs molecular mass (C) of the pyrolytic oxygenated compounds detected in the APCI(–) – FT-Orbitrap MS analysis.

oils have similar molecular characteristics. Three regions were identified in the diagrams according to the distinct compositional characteristics of some compound classes: sugar derivatives ($1.2 < H/C < 2.0$, $O/C > 0.5$), lipid derivatives ($1.6 < H/C < 2.0$, $O/C < 0.3$), and lignin derivatives – pyrolytic lignin ($0.4 < H/C < 1.5$, $O/C < 0.6$). The species with higher relative intensity in the LMM and HMM samples derived from SCB and SCS mainly concentrated in the region associated with pyrolytic lignin, an aromatic region with an H/C ratio mostly around 1.0 and acidic characteristics, therefore associated with monomeric and oligomeric phenolic compounds derived from lignin cracking[105].

In terms of molecular population density (Fig. 8-**B**), the species detected in all samples through the APCI(–) analysis predominantly grouped in the region of pyrolytic lignin, followed by the region associated with lipid derivatives and sugar derivatives. The higher density of compounds in the region associated with phenolics may be due to the greater ionization capacity of aromatic structures using the APCI source. Comparing the LMM with the HMM samples, a slight shift of the region with maximum kernel density to lower H/C and O/C values was observed in the HMM bio-oil fractions, which may indicate a more condensed and longer carbon chain character in the these samples compared to the LMM [106]. The main difference between the samples produced from different biomasses corresponds to compounds with lipid characteristics, wherein in the samples derived from SCS, a higher molecular population density was observed compared to those derived from SCB. This result, correlated with the data from the histograms in Fig. 7-**B**, indicates that the higher intensity of class O_2 in the SCS bio-oil fractions is due to a higher production of free fatty acids during the pyrolysis of this residual biomass, which suggests a greater availability of lipid constituents in the extractive fraction of SCS compared to SCB [10,107].

Through the trend lines of the O/C vs molecular mass plots shown in Fig. 8-**C,** where from left to right correspond to chemical species containing 1 to 10 oxygen atoms per structure, it was observed that the species present in the LMM fractions from both biomasses are distributed in monomer (100 to 250 Da), dimer (250 to 450 Da), and trimer (400 to 600 Da) structures, while the HMMs, on the other hand, also contained tetramers (550 to 750 Da) in their composition [108,109]. Since the number of oxygenated classes remains the same in both bio-oil fractions, the larger carbon chain size of the species presents in the HMM samples promoted the decrease of the O/C atomic ratio observed in the graphs of Fig. 7-**B**. The most intense molecules in the LMM-SCB and LMM-SCS samples corresponded to molecules of classes O_{1-4}, which had an O/C ratio < 0.6 and predominantly grouped in the region between 100 and 250 Da, corresponding to phenolic monomers. The most intense species in the HMM fractions corresponded to species containing 2 to 7 oxygen atoms and exhibited characteristics of lignin-derived species, grouping into regions of monomer, dimer, and trimer compounds. Comparing the samples produced from different feedstocks, it was observed that the distribution profiles of O/C vs molecular mass are similar between the correspondent LMM and HMM fractions from SCB and SCS pyrolysis. Based on the analysis in negative mode, it seems that the pyrolytic lignin derivatives were the main compounds found in both SCB and SCS bio-oil fractions. This suggests that similar phenolic compounds may have been produced during the pyrolysis of both biomasses, despite the higher lignin content in the sugarcane straw.

4. Conclusions

This research provides an in-depth evaluation of the potential for renewable energy generation and bio-inputs derived from the thermal conversion of sugarcane bagasse (SCB) and straw (SCS). The findings indicate that the residual biomass from the sugarcane industry possesses promising attributes for bioenergy production via the pyrolysis process. These attributes include a high holocellulose content, relatively low ash content, and a high heating value of $\sim$ 17 MJ kg^{-1}. The kinetic and thermodynamic studies unveiled activation energies between 125 and 160 kJ mol^{-1} for SCB pyrolysis and values between 140 and 290 kJ mol^{-1} for SCS thermal conversion. The pyrolysis of straw involved higher pre-exponential factors compared to bagasse, suggesting the presence of more intricate degradation mechanisms. However, for both types of biomasses evaluated, the potential energy barrier was relatively low (around 5 kJ mol^{-1}), signifying the high feasibility of the pyrolysis process for bio-product production. This conclusion was supported by the ΔG values, demonstrating that both SCB and SCS possess a high energy potential that can be harnessed in the form of pyrolytic products. The pyrolysis of bagasse and straw resulted in a high yield of liquid product (58–63 wt%), primarily composed of monomeric species distributed in sugar derivatives and phenolic compounds. The advanced characterization of the resulting liquid products revealed the predominance of oxygenated chemical species, containing between 1 and 10 oxygen atoms per structure. These species were grouped into characteristic regions of lignin derivatives and holocellulose-derived compounds. The correlation between the kinetic and thermodynamic results and the molecular characteristics of the products demonstrated that the residual biomasses of the sugarcane industry can have their chemical and energy potential repurposed through the production of a broad spectrum of renewable chemical inputs with diverse applications. In conclusion, the findings highlight the significant potential of bagasse and straw pyrolysis for energy recovery and the acquisition of value-added inputs such as bio-oil and biochar, which can broaden the product portfolio of the sugarcane sector.

CRediT authorship contribution statement

Tarcísio Martins: Writing – original draft, Methodology, Investigation, Formal analysis, Data curation. **Mirele Santana de Sá:** Formal analysis, Data curation. **Wenes Ramos Silva:** Investigation, Formal analysis, Data curation. **Caroline Carriel Schmitt:** Writing – review & editing, Supervision, Conceptualization. **Renata Moreira:** Supervision, Conceptualization. **Klaus Raffelt:** Writing – review & editing, Supervision, Resources, Project administration, Conceptualization. **Nicolaus Dahmen:** Supervision, Resources, Conceptualization. **Alberto Wisniewski:** Writing – review & editing, Supervision, Project administration, Methodology, Funding acquisition, Conceptualization.

Declaration of competing interest

The authors declare that they have no known competing financial interests or personal relationships that could have appeared to influence the work reported in this paper.

Data availability

No data was used for the research described in the article.

Acknowledgments

The authors are thankful to the analytical team of Karlsruhe Institute of Technology. We want to thank Capes for granting the scholarships and to CLQM (Center of Multi-users Chemistry Laboratories) from Federal University of Sergipe for the facilities.

References

[1] Toscano Miranda N, Lopes Motta I, Maciel Filho R, Wolf Maciel MR. Sugarcane bagasse pyrolysis: A review of operating conditions and products properties. Renew Sustain Energy Rev 2021;149:111394. https://doi.org/10.1016/j.rser.2021.111394.

[2] Li Z, Zhong Z, Yang Q, Ben H, Seufitelli GVS, Resende FLP. Parametric study of catalytic hydropyrolysis of rice husk over a hierarchical micro-mesoporous composite catalyst for production of light alkanes, alkenes, and liquid aromatic hydrocarbons. Fuel 2022;310:122457. https://doi.org/10.1016/j.fuel.2021.122457.

[3] Lu Q, Li W, Zhang X, Liu Z, Cao Q, Xie X, et al. Experimental study on catalytic pyrolysis of biomass over a Ni/Ca-promoted Fe catalyst. Fuel 2020;263:116690. https://doi.org/10.1016/j.fuel.2019.116690.

[4] Karimah A, Hani IK, Laksana RPB, Ismayati M, Solihat NN, Sari FP, et al. Extraction of lignin from sugarcane trash and its potency as biosurfactant. Bioresour Technol Reports 2023;24:101630. https://doi.org/10.1016/j.biteb.2023.101630.

[5] Eixenberger D, Carballo-Arce A-F, Vega-Baudrit J-R, Trimino-Vazquez H, Villegas-Peñaranda LR, Stöbener A, et al. Tropical agroindustrial biowaste revalorization through integrative biorefineries—review part II: pineapple, sugarcane and banana by-products in Costa Rica. Biomass Convers Biorefinery 2022. https://doi.org/10.1007/s13399-022-02721-9.

[6] Tramontina R, Scopel E, Brenelli L, Nogueira GP, Franco TT, Rezende CA, et al. Applying biorefinery concepts for sugarcane straw upcycling using alkaline and enzymatic treatments to produce value-added compounds and bioenergy. Biomass Bioenergy 2023;178:106972. https://doi.org/10.1016/j.biombioe.2023.106972.

[7] CONAB - Companhia Nacional de Abastecimento. Acompanhamento da safra brasileira de cana-de-açúcar: Safra 2023/24 2º Levantamento. vol. 8. Brasília, DF: 2023.

[8] Sganzerla WG, Lachos-Perez D, Buller LS, Zabot GL, Forster-Carneiro T. Cost analysis of subcritical water pretreatment of sugarcane straw and bagasse for second-generation bioethanol production: a case study in a sugarcane mill. Biofuels, Bioprod Biorefining 2022;16:435–50. https://doi.org/10.1002/bbb.2332.

[9] Negrão DR, Grandis A, Buckeridge MS, Rocha GJM, Leal MRLV, Driemeier C. Inorganics in sugarcane bagasse and straw and their impacts for bioenergy and biorefining: A review. Renew Sustain Energy Rev 2021;148:111268. https://doi.org/10.1016/j.rser.2021.111268.

[10] Najafi H, Golrokh Sani A, Sobati MA. A comparative evaluation on the physicochemical properties of sugarcane residues for thermal conversion processes. Ind Crops Prod 2023;202:117112. https://doi.org/10.1016/j.indcrop.2023.117112.

[11] Ong HC, Chen W-H, Singh Y, Gan YY, Chen C-Y, Show PL. A state-of-the-art review on thermochemical conversion of biomass for biofuel production: A TG-FTIR approach. Energy Convers Manag 2020;209:112634. https://doi.org/10.1016/j.enconman.2020.112634.
[12] Kumar R, Strezov V, Weldekidan H, He J, Singh S, Kan T, et al. Lignocellulose biomass pyrolysis for bio-oil production: A review of biomass pre-treatment methods for production of drop-in fuels. Renew Sustain Energy Rev 2020;123:109763. https://doi.org/10.1016/j.rser.2020.109763.
[13] Melikoglu M, Ozdemir M, Ates M. Pyrolysis kinetics, physicochemical characteristics and thermal decomposition behavior of agricultural wastes using thermogravimetric analysis. Energy Nexus 2023;11:100231. https://doi.org/10.1016/j.nexus.2023.100231.
[14] de Almeida SGC, Tarelho LAC, Hauschild T, Costa MAM, Dussán KJ. Biochar production from sugarcane biomass using slow pyrolysis: Characterization of the solid fraction. Chem Eng Process - Process Intensif 2022;179:109054. https://doi.org/10.1016/j.cep.2022.109054.
[15] Liu H, Zhang F, Liu H, Ma C, Hu J, Zhong W, et al. Comprehensive investigation on fast pyrolysis of waste Lotus shells to produce valuable products: Pyrolysis characteristics, reaction mechanism and economic analysis. J Environ Chem Eng 2023;11:111172. https://doi.org/10.1016/j.jece.2023.111172.
[16] K N Y, T PD, P S, S K, R YK, Varjani S, et al. Lignocellulosic biomass-based pyrolysis: A comprehensive review. Chemosphere 2022;286:131824. https://doi.org/10.1016/j.chemosphere.2021.131824.
[17] Stummann MZ, Høj M, Gabrielsen J, Clausen LR, Jensen PA, Jensen AD. A perspective on catalytic hydropyrolysis of biomass. Renew Sustain Energy Rev 2021;143:110960. https://doi.org/10.1016/j.rser.2021.110960.
[18] Liu S, Wu G, Gao Y, Li B, Feng Y, Zhou J, et al. Understanding the catalytic upgrading of bio-oil from pine pyrolysis over CO2-activated biochar. Renew Energy 2021;174:538–46. https://doi.org/10.1016/j.renene.2021.04.085.
[19] Ordonez-Loza J, Chejne F, Jameel AGA, Telalovic S, Arrieta AA, Sarathy SM. An investigation into the pyrolysis and oxidation of bio-oil from sugarcane bagasse: Kinetics and evolved gases using TGA-FTIR. J Environ Chem Eng 2021;9:106144. https://doi.org/10.1016/j.jece.2021.106144.
[20] Sharifzadeh M, Sadeqzadeh M, Guo M, Borhani TN, Murthy Konda NVSN, Garcia MC, et al. The multi-scale challenges of biomass fast pyrolysis and bio-oil upgrading: Review of the state of art and future research directions. Prog Energy Combust Sci 2019;71:1–80. https://doi.org/10.1016/j.pecs.2018.10.006.
[21] Zhong D, Zeng K, Li J, Qiu Y, Flamant G, Nzihou A, et al. Characteristics and evolution of heavy components in bio-oil from the pyrolysis of cellulose, hemicellulose and lignin. Renew Sustain Energy Rev 2022;157:111989. https://doi.org/10.1016/j.rser.2021.111989.
[22] Terrell E, Garcia-Perez M. Novel Strategy To Analyze Fourier Transform Ion Cyclotron Resonance Mass Spectrometry Data of Biomass Pyrolysis Oil for Oligomeric Structure Assignment. Energy Fuel 2020;34:8466–81. https://doi.org/10.1021/acs.energyfuels.0c01687.
[23] Staš M, Chudoba J, Auersvald M, Kubička D, Conrad S, Schulzke T, et al. Application of orbitrap mass spectrometry for analysis of model bio-oil compounds and fast pyrolysis bio-oils from different biomass sources. J Anal Appl Pyrolysis 2017;124:230–8. https://doi.org/10.1016/j.jaap.2017.02.002.
[24] Mase C, Hubert-Roux M, Afonso C, Giusti P. Contribution of atmospheric pressure chemical ionization mass spectrometry for the characterization of bio-oils from lignocellulosic biomass: Comparison with electrospray ionization and atmospheric pressure photoionization. J Anal Appl Pyrolysis 2022;167:105694. https://doi.org/10.1016/j.jaap.2022.105694.
[25] Hertzog J, Carré V, Le Brech Y, Dufour A, Aubriet F. Toward Controlled Ionization Conditions for ESI-FT-ICR-MS Analysis of Bio-Oils from Lignocellulosic Material. Energy Fuel 2016;30:5729–39. https://doi.org/10.1021/acs.energyfuels.6b00655.
[26] Carregosa ISC, Carregosa J de C, Silva WR, Santos TM, Wisniewski Jr A. Thermochemical conversion of aquatic weed biomass in a rotary kiln reactor for production of bio-based derivatives. J Anal Appl Pyrolysis 2023;173:106048. https://doi.org/10.1016/j.jaap.2023.106048.
[27] Crepier J, Le Masle A, Charon N, Albrieux F, Duchene P, Heinisch S. Ultra-high performance supercritical fluid chromatography hyphenated to atmospheric pressure chemical ionization high resolution mass spectrometry for the characterization of fast pyrolysis bio-oils. J Chromatogr B 2018;1086:38–46. https://doi.org/10.1016/j.jchromb.2018.04.005.
[28] Wang J, Yellezuome D, Zhang Z, Liu S, Lu J, Zhang P, et al. Understanding pyrolysis mechanisms of pinewood sawdust and sugarcane bagasse from kinetics and thermodynamics. Ind Crops Prod 2022;177:114378. https://doi.org/10.1016/j.indcrop.2021.114378.
[29] Shagali AA, Mostafa ME, Li H, Hu S, Xu J, Jiang L, et al. Pyrolysis characteristics and kinetic parameters assessment of typical agricultural residues using high heating photothermal TGA. J Anal Appl Pyrolysis 2023;174:106109. https://doi.org/10.1016/j.jaap.2023.106109.
[30] Choudhury ND, Bhuyan N, Bordoloi N, Saikia N, Kataki R. Production of bio-oil from coir pith via pyrolysis: kinetics, thermodynamics, and optimization using response surface methodology. Biomass Convers Biorefinery 2021;11:2881–98. https://doi.org/10.1007/s13399-020-00630-3.
[31] Santos VO, Araujo RO, Ribeiro FCP, Queiroz LS, Guimarães MN, Colpani D, et al. Non-isothermal kinetics evaluation of buriti and inaja seed biomass waste for pyrolysis thermochemical conversion technology. Biomass Convers Biorefinery 2023;13:10893–909. https://doi.org/10.1007/s13399-021-01922-y.
[32] Alabi AO, Sambo AS. Comparative bio-energy potential of De-oiled coconut pulp and Coconut shell: Insights from physicochemical characterization, pyrolysis kinetics and thermodynamic studies. Fuel Process Technol 2023;243:107658. https://doi.org/10.1016/j.fuproc.2023.107658.
[33] Alashmawy MM, Hassan HS, Ookawara SA, Elwardany AE. Thermal decomposition characteristics and study of the reaction kinetics of tea-waste. Biomass Convers Biorefinery 2023;13:9487–505. https://doi.org/10.1007/s13399-023-04017-y.
[34] Rodríguez-Machín L, Arteaga-Pérez LE, Manrique R, Pala M, Feys J, Ghysels S, et al. The effect of citric acid pretreatment on composition and stability of bio-oil from sugar cane residues using a continuous lab-scale pyrolysis reactor. J Anal Appl Pyrolysis 2023;175:106183. https://doi.org/10.1016/j.jaap.2023.106183.
[35] Barros JAS, Krause MC, Lazzari E, Bjerk TR, do Amaral Al, Caramão EB, et al. Chromatographic characterization of bio-oils from fast pyrolysis of sugar cane residues (straw and bagasse) from four genotypes of the Saccharum Complex. Microchem J 2018;137:30–6. https://doi.org/10.1016/j.microc.2017.09.015.
[36] Song F, Li T, Zhang J, Wang X, Bai Y, Giesy JP, et al. Novel Insights into the Kinetics, Evolved Gases, and Mechanisms for Biomass (Sugar Cane Residue) Pyrolysis. Environ Sci Technol 2019;53:13495–505. https://doi.org/10.1021/acs.est.9b04595.
[37] Rueda-Ordóñez YJ, Tannous K. Isoconversional kinetic study of the thermal decomposition of sugarcane straw for thermal conversion processes. Bioresour Technol 2015;196:136–44. https://doi.org/10.1016/j.biortech.2015.07.062.
[38] de Palma KR, García-Hernando N, Silva MA, Tomaz E, Soria-Verdugo A. Pyrolysis and Combustion Kinetic Study and Complementary Study of Ash Fusibility Behavior of Sugarcane Bagasse, Sugarcane Straw, and Their Pellets—Case Study of Agro-Industrial Residues. Energy Fuel 2019;33:3227–38. https://doi.org/10.1021/acs.energyfuels.8b04288.
[39] Kim H, Yu S, Kim M, Ryu C. Progressive deconvolution of biomass thermogram to derive lignocellulosic composition and pyrolysis kinetics for parallel reaction model. Energy 2022;254:124446. https://doi.org/10.1016/j.energy.2022.124446.
[40] Manuel Rêgo Silva J, de Morais M, Araújo A, da Costa P, Evangelista J, Ribeiro da Silva D, et al. Evaluation of the kinetic and thermodynamic parameters in catalytic pyrolysis process of sunflower oil using Al-MCM-41 and zeolite H-ZSM-5. Fuel 2023;333:126225. https://doi.org/10.1016/j.fuel.2022.126225.
[41] Zhang Z, Li Y, Luo L, Yellezuome D, Rahman MM, Zou J, et al. Insight into kinetic and Thermodynamic Analysis methods for lignocellulosic biomass pyrolysis. Renew Energy 2023;202:154–71. https://doi.org/10.1016/j.renene.2022.11.072.
[42] Santos TM, da Silva WR, Carregosa JC, Schmitt CC, Moreira R, Raffelt K, et al. Thermal Conversion of Sugarcane Bagasse Coupled with Vapor Phase Hydrotreatment over Nickel-Based Catalysts: A Comprehensive Characterization of Upgraded Products. Catalysts 2022:12. https://doi.org/10.3390/catal12040355.
[43] Silva WR, Carregosa J de C, Almeida-Couto JMF, Cardozo-Filho L, Wisniewski A. Management of de-oiled coffee beans biomass through pyrolysis process: Towards a circular bioeconomy. J Anal Appl Pyrolysis 2022;168:105763. https://doi.org/10.1016/j.jaap.2022.105763.
[44] Onokwai A, Ajisegiri ESA, Okokpujie IP, Ibikunle RA, Oki M, Dirisu JO. Characterization of lignocellulose biomass based on proximate, ultimate, structural composition, and thermal analysis. Mater Today Proc 2022;65:2156–62. https://doi.org/10.1016/j.matpr.2022.05.313.
[45] Noushabadi AS, Dashti A, Ahmadijokani F, Hu J, Mohammadi AH. Estimation of higher heating values (HHVs) of biomass fuels based on ultimate analysis using machine learning techniques and improved equation. Renew Energy 2021;179:550–62. https://doi.org/10.1016/j.renene.2021.07.003.
[46] Singh RK, Pandey D, Patil T, Sawarkar AN. Pyrolysis of banana leaves biomass: Physico-chemical characterization, thermal decomposition behavior, kinetic and thermodynamic analyses. Bioresour Technol 2020;310:123464. https://doi.org/10.1016/j.biortech.2020.123464.
[47] Silva JE, Calixto GQ, de Almeida CC, Melo DMA, Melo MAF, Freitas JCO, et al. Energy potential and thermogravimetric study of pyrolysis kinetics of biomass wastes. J Therm Anal Calorim 2019;137:1635–43. https://doi.org/10.1007/s10973-019-08048-4.
[48] Couhert C, Commandre J-M, Salvador S. Is it possible to predict gas yields of any biomass after rapid pyrolysis at high temperature from its composition in cellulose, hemicellulose and lignin? Fuel 2009;88:408–17. https://doi.org/10.1016/j.fuel.2008.09.019.
[49] Demirbaş A. Relationships between lignin contents and fixed carbon contents of biomass samples. Energy Convers Manag 2003;44:1481–6. https://doi.org/10.1016/S0196-8904(02)00168-1.
[50] Barros JAS, Schneider JK, Farrapeira RO, Andrade YB, Krause LC, Bjerk TR, et al. Recovery of waste biomass: pyrolysis and characterization of sugarcane residues and their bio-oils. Biofuels 2022;13:843–52. https://doi.org/10.1080/17597269.2021.1992954.
[51] Reyes L, Abdelouahed L, Mohabeer C, Buvat J-C, Taouk B. Energetic and exergetic study of the pyrolysis of lignocellulosic biomasses, cellulose, hemicellulose and lignin. Energy Convers Manag 2021;244:114459. https://doi.org/10.1016/j.enconman.2021.114459.
[52] Liew YW, Arumugasamy SK, Selvarajoo A. Potential of Biochar as Soil Amendment: Prediction of Elemental Ratios from Pyrolysis of Agriculture Biomass Using Artificial Neural Network. Water, Air, Soil Pollut 2022;233:54. https://doi.org/10.1007/s11270-022-05510-2.
[53] Alves JLF, da Silva JCG, Mumbach GD, Alves RF, Di Domenico M, Marangoni C. Physicochemical properties, pyrolysis kinetics, thermodynamic parameters of activation, and evolved volatiles of mango seed waste as a bioenergy feedstock: A

potential exploration. Thermochim Acta 2023;725:179519. https://doi.org/10.1016/j.tca.2023.179519.
[54] Chen N, Pilla S. A comprehensive review on transforming lignocellulosic materials into biocarbon and its utilization for composites applications. Compos Part C Open Access 2022;7:100225. https://doi.org/10.1016/j.jcomc.2021.100225.
[55] Kumar M, Upadhyay SN, Mishra PK. A comparative study of thermochemical characteristics of lignocellulosic biomasses. Bioresour Technol Reports 2019;8:100186. https://doi.org/10.1016/j.biteb.2019.100186.
[56] Athira G, Bahurudeen A, Appari S. Thermochemical Conversion of Sugarcane Bagasse: Composition, Reaction Kinetics, and Characterisation of By-Products. Sugar Tech 2021;23:433–52. https://doi.org/10.1007/s12355-020-00865-4.
[57] Liu C, Wang H, Karim AM, Sun J, Wang Y. Catalytic fast pyrolysis of lignocellulosic biomass. Chem Soc Rev 2014;43:7594–623. https://doi.org/10.1039/C3CS60414D.
[58] Rego F, Soares Dias AP, Casquilho M, Rosa FC, Rodrigues A. Fast determination of lignocellulosic composition of poplar biomass by thermogravimetry. Biomass Bioenergy 2019;122:375–80. https://doi.org/10.1016/j.biombioe.2019.01.037.
[59] Dhyani V, Bhaskar T. A comprehensive review on the pyrolysis of lignocellulosic biomass. Renew Energy 2018;129:695–716. https://doi.org/10.1016/j.renene.2017.04.035.
[60] Zong P, Jiang Y, Tian Y, Li J, Yuan M, Ji Y, et al. Pyrolysis behavior and product distributions of biomass six group components: Starch, cellulose, hemicellulose, lignin, protein and oil. Energy Convers Manag 2020;216:112777. https://doi.org/10.1016/j.enconman.2020.112777.
[61] Dhyani V, Bhaskar T. Kinetic Analysis of Biomass Pyrolysis. Waste Biorefinery, Elsevier 2018:39–83. https://doi.org/10.1016/B978-0-444-63992-9.00002-1.
[62] Singh B, Singh S, Kumar P. In-depth analyses of kinetics, thermodynamics and solid reaction mechanism for pyrolysis of hazardous petroleum sludge based on isoconversional models for its energy potential. Process Saf Environ Prot 2021;146:85–94. https://doi.org/10.1016/j.psep.2020.08.038.
[63] Wang S, Lin H, Ru B, Dai G, Wang X, Xiao G, et al. Kinetic modeling of biomass components pyrolysis using a sequential and coupling method. Fuel 2016;185:763–71. https://doi.org/10.1016/j.fuel.2016.08.037.
[64] Chen D, Cen K, Zhuang X, Gan Z, Zhou J, Zhang Y, et al. Insight into biomass pyrolysis mechanism based on cellulose, hemicellulose, and lignin: Evolution of volatiles and kinetics, elucidation of reaction pathways, and characterization of gas, biochar and bio-oil. Combust Flame 2022;242:112142. https://doi.org/10.1016/j.combustflame.2022.112142.
[65] Qiao Y, Wang B, Ji Y, Xu F, Zong P, Zhang J, et al. Thermal decomposition of castor oil, corn starch, soy protein, lignin, xylan, and cellulose during fast pyrolysis. Bioresour Technol 2019;278:287–95. https://doi.org/10.1016/j.biortech.2019.01.102.
[66] Ben Abdallah A, Ben Hassen Trabelsi A, Navarro MV, Veses A, García T, Mihoubi D. Pyrolysis of tea and coffee wastes: effect of physicochemical properties on kinetic and thermodynamic characteristics. J Therm Anal Calorim 2023;148:2501–15. https://doi.org/10.1007/s10973-022-11878-4.
[67] Xiao R, Yang W, Cong X, Dong K, Xu J, Wang D, et al. Thermogravimetric analysis and reaction kinetics of lignocellulosic biomass pyrolysis. Energy 2020;201:117537. https://doi.org/10.1016/j.energy.2020.117537.
[68] Chua YW, Wu H, Yu Y. Effect of cellulose–lignin interactions on char structural changes during fast pyrolysis at 100–350 °C. Proc Combust Inst 2021;38:3977–86. https://doi.org/10.1016/j.proci.2020.08.014.
[69] Braga RM, Melo DMA, Aquino FM, Freitas JCO, Melo MAF, Barros JMF, et al. Characterization and comparative study of pyrolysis kinetics of the rice husk and the elephant grass. J Therm Anal Calorim 2014;115:1915–20. https://doi.org/10.1007/s10973-013-3503-7.
[70] Dong R, Chen F, Zhang F, Yang S, Liu H, Wang H, et al. A comprehensive evaluation on pyrolysis kinetics, thermodynamics, product properties and formation pathways of jatropha oil for high-value utilization. Fuel 2022;313:122982. https://doi.org/10.1016/j.fuel.2021.122982.
[71] Vyazovkin S, Burnham AK, Criado JM, Pérez-Maqueda LA, Popescu C, Sbirrazzuoli N. ICTAC Kinetics Committee recommendations for performing kinetic computations on thermal analysis data. Thermochim Acta 2011;520:1–19. https://doi.org/10.1016/j.tca.2011.03.034.
[72] Colpani D, Santos VO, Araujo RO, Lima VMR, Tenório JAS, Coleti J, et al. Bioenergy potential analysis of Brazil nut biomass residues through pyrolysis: Gas emission, kinetics, and thermodynamic parameters. Clean Chem Eng 2022;1:100002. https://doi.org/10.1016/j.clce.2022.100002.
[73] Nishu LC, Yellezuome D, Li Y, Liu R. Catalytic pyrolysis of rice straw for high yield of aromatics over modified ZSM-5 catalysts and its kinetics. Renew. Energy 2023;209:569–80. https://doi.org/10.1016/j.renene.2023.04.025.
[74] Iffah Farhah Mohd Yusof N, Aqilah Shamsuddin N, Aini Zakaria H, Farizan Munajat N. Exploring the potential of fish waste (Sardinella fimbriata) through pyrolysis: A study of kinetics and thermodynamics using isoconversional methods. Mater Sci Energy Technol 2023;6:460–71. https://doi.org/10.1016/j.mset.2023.04.009.
[75] Chen P, Hu C, Gu J, Lin X, Yang C, Leu S-Y, et al. Pyrolysis characteristics of tea oil camellia (Camellia oleifera Abel.) shells and their chemically pre-treated residues: Kinetics, mechanisms, product evaluation and joint optimization. J Anal Appl Pyrolysis 2022;164:105526. https://doi.org/10.1016/j.jaap.2022.105526.
[76] Alves JLF, da Silva JCG, Mumbach GD, Arias S, Pacheco JGA, Di Domenico M, et al. Valorization of royal palm tree agroindustrial waste via pyrolysis with a focus on physicochemical properties, kinetic triplet, thermodynamic parameters, and volatile products. Biomass Bioenergy 2023;177:106937. https://doi.org/10.1016/j.biombioe.2023.106937.
[77] He Y, Chang C, Li P, Han X, Li H, Fang S, et al. Thermal decomposition and kinetics of coal and fermented cornstalk using thermogravimetric analysis. Bioresour Technol 2018;259:294–303. https://doi.org/10.1016/j.biortech.2018.03.043.
[78] Li C, Li L, Yellezuome D, Cai J, Liu R, Hu J. Physicochemical investigation and thermogravimetric analysis of bamboo and poplar wood residues and tire rubber waste: Kinetic and thermodynamic analyses. Ind Crops Prod 2023;206:117715. https://doi.org/10.1016/j.indcrop.2023.117715.
[79] Saracoglu MS, Coruh MK. Thermal degradation properties, kinetic, thermodynamic and reaction mechanism of pyrolysis of biomass shells: pistachio, almond, walnut and hazelnut as bioenergy potential. Biomass Convers Biorefinery 2023. https://doi.org/10.1007/s13399-023-05052-5.
[80] Xiong Z, Xiong Y, Li Q, Han H, Deng W, Xu J, et al. Effects of vapor-/solid-phase interactions among cellulose, hemicellulose and lignin on the formation of heavy components in bio-oil during pyrolysis. Fuel Process Technol 2022;225:107042. https://doi.org/10.1016/j.fuproc.2021.107042.
[81] Qiu Y, Zhong D, Zeng K, Li J, Flamant G, Nzihou A, et al. Effects of cellulose-lignin interaction on the evolution of biomass pyrolysis bio-oil heavy components. Fuel 2022;323:124413. https://doi.org/10.1016/j.fuel.2022.124413.
[82] Cai Q, Gong T, Yu T, Zhang S. Comparison of hydrocracking and cracking of pyrolytic lignin over different Ni-based catalysts for light aromatics production. Fuel Process Technol 2023;240:107564. https://doi.org/10.1016/j.fuproc.2022.107564.
[83] Yang H, Yan R, Chen H, Zheng C, Lee DH, Liang DT. In-Depth Investigation of Biomass Pyrolysis Based on Three Major Components: Hemicellulose. Cellulose and Lignin Energy & Fuels 2006;20:388–93. https://doi.org/10.1021/ef0580117.
[84] Tsekos C, Tandurella S, de Jong W. Estimation of lignocellulosic biomass pyrolysis product yields using artificial neural networks. J Anal Appl Pyrolysis 2021;157:105180. https://doi.org/10.1016/j.jaap.2021.105180.
[85] Chen D, Xu J, Ling P, Fang Z, Ren Q, Xu K, et al. Formation and evolution mechanism of persistent free radicals in biochar during biomass pyrolysis: Insights from biochar's element composition and chemical structure. Fuel 2024;357:129910. https://doi.org/10.1016/j.fuel.2023.129910.
[86] Anand A, Gautam S, Ram LC. Feedstock and pyrolysis conditions affect suitability of biochar for various sustainable energy and environmental applications. J Anal Appl Pyrolysis 2023;170:105881. https://doi.org/10.1016/j.jaap.2023.105881.
[87] Riaz M, Khan M, Ali S, Khan MD, Ahmad R, Khan MJ, et al. Sugarcane waste straw biochar and its effects on calcareous soil and agronomic traits of okra. Arab J Geosci 2018;11:752. https://doi.org/10.1007/s12517-018-4113-2.
[88] Wang Q, Li Y, Yu Z, Li X, Yin S, Ji W, et al. Highly porous carbon derived from hydrothermal-pyrolysis synergistic carbonization of biomass for enhanced CO2 capture. Colloids Surfaces A Physicochem Eng Asp 2023;673:131787. https://doi.org/10.1016/j.colsurfa.2023.131787.
[89] Sharma P, Sharma S, Sharma SK, Jain A, Shrivastava K. Review on recent advancement of adsorption potential of sugarcane bagasse biochar in wastewater treatment. Chem Eng Res Des 2024;206:428–39. https://doi.org/10.1016/j.cherd.2024.04.055.
[90] Kim M, Fernando JFS, Li Z, Alowasheeir A, Ashok A, Xin R, et al. Ultra-stable sodium ion storage of biomass porous carbon derived from sugarcane. Chem Eng J 2022;445:136344. https://doi.org/10.1016/j.cej.2022.136344.
[91] Ansari KB, Arora JS, Chew JW, Dauenhauer PJ, Mushrif SH. Fast Pyrolysis of Cellulose, Hemicellulose, and Lignin: Effect of Operating Temperature on Bio-oil Yield and Composition and Insights into the Intrinsic Pyrolysis Chemistry. Ind Eng Chem Res 2019;58:15838–52. https://doi.org/10.1021/acs.iecr.9b00920.
[92] Machado H, Cristino AF, Orišková S, Galhano dos Santos R. Bio-Oil: The Next-Generation Source of Chemicals. Reactions 2022;3:118–37. https://doi.org/10.3390/reactions3010009.
[93] Cole DP, Smith EA, Dalluge D, Wilson DM, Heaton EA, Brown RC, et al. Molecular characterization of nitrogen-containing species in switchgrass bio-oils at various harvest times. Fuel 2013;111:718–26. https://doi.org/10.1016/j.fuel.2013.04.064.
[94] Szczerbowski D, Pitarelo AP, Zandoná Filho A, Ramos LP. Sugarcane biomass for biorefineries: Comparative composition of carbohydrate and non-carbohydrate components of bagasse and straw. Carbohydr Polym 2014;114:95–101. https://doi.org/10.1016/j.carbpol.2014.07.052.
[95] Xu K, Li J, Zeng K, Zhong D, Peng J, Qiu Y, et al. The characteristics and evolution of nitrogen in bio-oil from microalgae pyrolysis in molten salt. Fuel 2023;331:125903. https://doi.org/10.1016/j.fuel.2022.125903.
[96] Cui D, Li J, Zhang X, Zhang L, Chang H, Wang Q. Pyrolysis temperature effect on compositions of basic nitrogen species in Huadian shale oil using positive-ion ESI FT-ICR MS and GC-NCD. J Anal Appl Pyrolysis 2021;153:104980. https://doi.org/10.1016/j.jaap.2020.104980.
[97] Michailof CM, Kalogiannis KG, Sfetsas T, Patiaka DT, Lappas AA. Advanced analytical techniques for bio-oil characterization. WIREs Energy Environ 2016;5:614–39. https://doi.org/10.1002/wene.208.
[98] Chacón-Patiño ML, Mase C, Maillard JF, Barrère-Mangote C, Dayton DC, Afonso C, et al. Petroleomics Approach to Investigate the Composition of Upgrading Products from Pyrolysis Bio-Oils as Determined by High-Field FT-ICR MS. Energy Fuel 2023. https://doi.org/10.1021/acs.energyfuels.3c02599.
[99] Qiu Y, Zhong D, Zeng K, Li J, Yang H, Chen H. Evolution of lignin pyrolysis heavy components through the study of representative lignin monomers. Fuel Process Technol 2023;250:107910. https://doi.org/10.1016/j.fuproc.2023.107910.
[100] Hertzog J, Carré V, Jia L, Mackay CL, Pinard L, Dufour A, et al. Catalytic Fast Pyrolysis of Biomass over Microporous and Hierarchical Zeolites: Characterization of Heavy Products. ACS Sustain Chem Eng 2018;6:4717–28. https://doi.org/10.1021/acssuschemeng.7b03837.

[101] Stankovikj F, McDonald AG, Helms GL, Garcia-Perez M. Quantification of Bio-Oil Functional Groups and Evidences of the Presence of Pyrolytic Humins. Energy Fuel 2016;30:6505–24. https://doi.org/10.1021/acs.energyfuels.6b01242.
[102] Palazzolo MA, Garcia-Perez M. Microbial lipid biosynthesis from lignocellulosic biomass pyrolysis products. Biotechnol Adv 2022;54:107791. https://doi.org/10.1016/j.biotechadv.2021.107791.
[103] Patwardhan PR, Dalluge DL, Shanks BH, Brown RC. Distinguishing primary and secondary reactions of cellulose pyrolysis. Bioresour Technol 2011;102:5265–9. https://doi.org/10.1016/j.biortech.2011.02.018.
[104] Wang Y, Agarwal S, Tang Z, Heeres HJ. Exploratory catalyst screening studies on the liquefaction of model humins from C6 sugars. RSC Adv 2017;7:5136–47. https://doi.org/10.1039/C6RA24218A.
[105] Reymond C, Dubuis A, Le Masle A, Colas C, Chahen L, Destandau E, et al. Characterization of liquid–liquid extraction fractions from lignocellulosic biomass by high performance liquid chromatography hyphenated to tandem high-resolution mass spectrometry. J Chromatogr A 2020;1610:460569. https://doi.org/10.1016/j.chroma.2019.460569.
[106] Xiong Z, Guo J, Han H, Xu J, Jiang L, Su S, et al. Effects of AAEMs on formation of heavy components in bio-oil during pyrolysis at various temperatures and heating rates. Fuel Process Technol 2021;213:106690. https://doi.org/10.1016/j.fuproc.2020.106690.
[107] del Río JC, Lino AG, Colodette JL, Lima CF, Gutiérrez A, Martínez ÁT, et al. Differences in the chemical structure of the lignins from sugarcane bagasse and straw. Biomass Bioenergy 2015;81:322–38. https://doi.org/10.1016/j.biombioe.2015.07.006.
[108] Prothmann J, Spégel P, Sandahl M, Turner C. Identification of lignin oligomers in Kraft lignin using ultra-high-performance liquid chromatography/high-resolution multiple-stage tandem mass spectrometry (UHPLC/HRMSn). Anal Bioanal Chem 2018;410:7803–14. https://doi.org/10.1007/s00216-018-1400-4.
[109] Asare SO, Huang F, Lynn BC. Characterization and sequencing of lithium cationized β-O-4 lignin oligomers using higher-energy collisional dissociation mass spectrometry. Anal Chim Acta 2019;1047:104–14. https://doi.org/10.1016/j.aca.2018.09.068.